

Riemannian Geometry of Resonant Optical Responses

Junyeong Ahn,^{1,*} Guang-Yu Guo,^{2,3,†} Naoto Nagaosa,^{4,5,‡} and Ashvin Vishwanath^{1,§}

¹*Department of Physics, Harvard University, Cambridge, MA 02138, USA*

²*Department of Physics and Center for Theoretical Physics, National Taiwan University, Taipei 10617, Taiwan*

³*Physics Division, National Center for Theoretical Sciences, Taipei 10617, Taiwan*

⁴*RIKEN Center for Emergent Matter Science (CEMS), Wako, Saitama 351-0198, Japan*

⁵*Department of Applied Physics, The University of Tokyo, Bunkyo, Tokyo 113-8656, Japan*

(Dated: December 23, 2024)

Geometry of quantum states has proved to be a useful concept for understanding responses of electronic systems to static electromagnetic fields [1–15], as exemplified by the quantum and anomalous Hall effects [1–4]. However, it has been challenging to relate quantum geometry with resonant optical responses. The main obstacle is that optical transitions are properties of a pair of states, while existing geometrical properties are defined for a single state. Therefore, concrete geometric understanding of optical responses has been limited to two-level systems [16–18], where one of two states determines the Hilbert space completely. Here, we construct a general theory of Riemannian geometry for resonant optical processes, by identifying transition dipole moment matrix elements as tangent vectors. This theory applies to arbitrarily high-order responses, suggesting that optical responses can be generally thought of as manifestations of the Riemannian geometry of quantum states. We use our theory to show that third-order photovoltaic Hall effects are related to the Riemann curvature tensor and demonstrate an experimentally accessible regime where they dominate the response.

A common feature of geometric responses is that they originate from inter-band hybridizations, such that they appear as quantum corrections to semiclassical descriptions. Since resonant optical responses are inherently inter-band quantum-mechanical processes, they are ideal candidates for a geometrical interpretation. Indeed, nonlinear optical responses, in particular, have attracted much attention recently for this reason [16–23] in addition to the possibility of diverse physical applications [24–26]. Quantized injection photocurrent responses were found in chiral semimetals [16, 17], and the shift photovoltaic responses of semimetals have been found to be described by the Levi-Civita connection [18], a geometric quantity distinguished from the typical Berry curvature and quantum metric.

However, the study of the relationship between quantum geometry and optical responses has been limited to the vicinity of band-crossing points in semimetals, where two-band descriptions are good approximations [16–18]. The fundamental reason for this is the absence of a proper theory explaining the geometry of optical transitions; the geometric quantities like

the quantum metric and the Berry curvature are usually defined for a single quantum state [27], while optical transitions involve a pair of states. While the wave function of one state completely determines the other in two-band systems, in general the two quantum states involved in an optical transition are independent, meaning that the geometry of a pair of states is different from the geometry of a single state.

In this Letter, we introduce a general theoretical description of the Riemannian geometry for resonant optical transitions. We consider independent electronic quasiparticles at zero-temperature in clean crystals and neglect photon momentum. Let us note that optical responses are described by the electric dipole Hamiltonian [28, 29]

$$\hat{H}_{\text{int}} = e\mathbf{E}(t) \cdot \hat{\mathbf{r}}, \quad (1)$$

where $-e$ is the electric charge (Methods 1 summarizes our conventions and definitions), and $\hat{\mathbf{r}}$ is the position operator of electrons, and $\mathbf{E}(t)$ is the external electric field. Since all information on the unperturbed quantum states is encoded in the overlap matrices $\langle \psi_{m\mathbf{k}} | H_{\text{int}} | \psi_{n\mathbf{k}} \rangle$ in perturbative response theory, the transition dipole moment matrix element (per unit charge)

$$\mathbf{r}_{mn}(\mathbf{k}) = \langle \psi_{m\mathbf{k}} | \hat{\mathbf{r}} | \psi_{n\mathbf{k}} \rangle \quad (2)$$

is the fundamental building block of the k th-order nonlinear optical conductivity tensors [26] defined by (see Methods 2)

$$j^a(\omega) = \sum_k \sum_{a_i, \omega_i} \sigma^{a; a_1, \dots, a_k}(\omega; \omega_1, \dots, \omega_k) E^{a_1}(\omega_1) \dots E^{a_k}(\omega_k). \quad (3)$$

Our key observation is that the transition dipole moment matrix elements define tangent vectors on the manifold of quantum states. In differential geometry, the tangent vector associated with a coordinate k^a is written in an abstract way as $\frac{\partial}{\partial k^a}$ for $a = 1, \dots, d$, where d is the spatial dimension. Therefore, one can expect that the position operator $\hat{r}^a \sim i\partial_a \equiv i\frac{\partial}{\partial k^a}$ defines the tangent vector for the momentum coordinate k^a defined on a manifold. Then, defining a metric tensor defines the Riemannian structure. We make this idea concrete for the representation of \hat{r}^a on the cell-periodic Bloch states. The same procedure may also be applied to the energy eigenstates in a $\mathbf{k} \cdot \mathbf{p}$ model or a tight-binding model.

This construction allows us to show that resonant optical responses are geometric in nature. We show that linear optical responses and second-order bulk photovoltaic effects are

* junyeongahn@fas.harvard.edu

† gyguo@phys.ntu.edu.tw

‡ nagaosa@riken.jp

§ avishwanath@g.harvard.edu

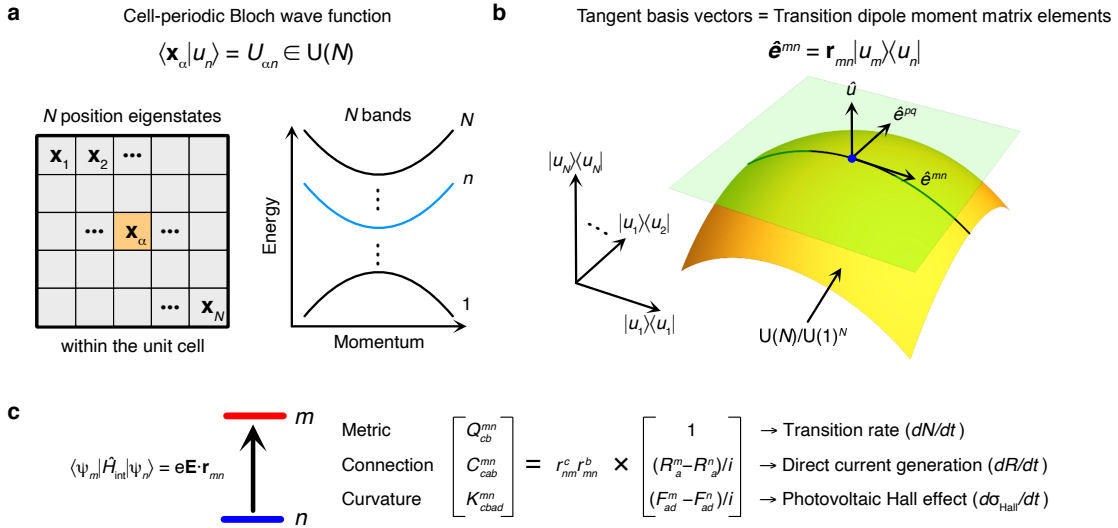


FIG. 1: Geometry of the cell-periodic Bloch state and optical transitions. **a**, Cell-periodic Bloch wave function as an N by N unitary matrix. The limit $N \rightarrow \infty$ is assumed. **b**, Transition dipole moment matrix elements as tangent basis vectors. \hat{e}^{pq} s and \hat{e}^{mn} are tangent vectors on the manifold $U(N)/U(1)^N$ of cell-periodic Bloch states, and \hat{u} presents normal vectors. Here, $U(1)^N$ corresponds to the gauge degrees of freedom. Optical transitions between m and n states reveal geometrical information on the curve generated by \hat{e}^{mn} . **c**, Physical meaning of the Hermitian metric, connection, and curvature in optical processes for non-degenerate states. R_a^n and F_{ad}^n are the Wannier center and the Berry curvature of the state $|u_n\rangle$.

manifestations of the metric and connection. In particular, the non-quantized injection photocurrents in chiral semimetals due to higher-band corrections to the two-band description [16, 17] can still be regarded as geometric responses, although not as topological responses. Furthermore, our geometric perspective can serve as a useful organizing principle for more complicated higher-order optical conductivity tensors. As an example, we show that Riemann curvature characterizes the third-order photovoltaic Hall conductivity near the band edge of gapped topological materials.

To simplify the presentation of our theory, we mainly consider non-degenerate states without spacetime inversion symmetry in the main text. See Methods 5 and 6 for details on degenerate states and symmetry constraints.

We begin by revisiting the geometric meaning of the position operator. The position operator is represented in the Bloch state basis as [30, 31]

$$r_{mn}^a(\mathbf{k}) = \delta_{mn} i\partial_a + \langle u_{m\mathbf{k}} | i\partial_a | u_{n\mathbf{k}} \rangle. \quad (4)$$

The second term is a geometric quantity widely known as the non-abelian Berry connection. Here, instead of viewing it as a connection, we regard it as the Maurer-Cartan form $\xi_a(\mathbf{k}) = U^\dagger(\mathbf{k}) i\partial_a U(\mathbf{k})$ (see Methods 4) of the $N \times N$ unitary matrix $U_{\alpha m}(\mathbf{k}) = \langle x_\alpha | u_{m\mathbf{k}} \rangle$, where $|x_\alpha\rangle$ is a position eigenstate within the unit cell with eigenvalue x_α . Here, we take both the number of bands and the number of position eigenstates in the unit cell to be a finite number N for definiteness [Fig. 1(a)]. The limit $N \rightarrow \infty$ is taken in the end. The Maurer-Cartan form has one-to-one correspondence with the tangent vector $i\partial_a U(\mathbf{k})$ at $U(\mathbf{k})$, so it can be simply regarded as a tangent vector. After modding out the $U(1)$ gauge degrees of freedom of each state from $U(N)$,

we obtain the manifold $\mathcal{M} = U(N)/U(1)^N$ of the cell-periodic Bloch states. The tangent vectors in \mathcal{M} are given $\xi_a^{\mathcal{M}}(\mathbf{k}) = U^\dagger(\mathbf{k}) i\partial_a U(\mathbf{k}) - U^\dagger(\mathbf{k}) i\partial_a U(\mathbf{k})|_{U(1)^N}$, where $[U^\dagger(\mathbf{k}) i\partial_a U(\mathbf{k})|_{U(1)^N}]_{mn} = \delta_{mn} \langle u_{m\mathbf{k}} | i\partial_a | u_{n\mathbf{k}} \rangle$ is the projection of ξ_a along the $U(1)^N$ direction. In the operator form, the tangent vector is $\hat{\xi}_a^{\mathcal{M}}(\mathbf{k}) = \sum_{m \neq n} r_{mn}^a(\mathbf{k}) |u_{m\mathbf{k}}\rangle \langle u_{n\mathbf{k}}|$.

Now we arrive at our main result; the transition dipole moment r_{mn}^a between m and n states is one particular component of the $N(N-1)/2$ -dimensional complex-valued tangent vector $\hat{e}_a^{\mathcal{M}}$ (i.e., r_{mn}^a is a vielbein). Namely, an optical transition between m and n states probes the one-dimensional complex vector space spanned by

$$\hat{e}_a^{mn}(\mathbf{k}) \equiv r_{mn}^a(\mathbf{k}) |u_{m\mathbf{k}}\rangle \langle u_{n\mathbf{k}}|, \quad a = 1, \dots, d, \quad (5)$$

with given m and n with $m \neq n$ [Fig. 1(b)]. In the following, we describe the Riemannian structure of the subspace spanned by \hat{e}_a^{mn} s. Here, at most two $\hat{e}_{a=1, \dots, d}^{mn}$ s are linearly independent for a given pair (m, n) because one complex dimension is fully covered by two independent real coordinates.

The complex Riemannian structure is induced by the natural inner product in the space of $N \times N$ matrices, called the Hilbert-Schmidt inner product:

$$(A, B) = \sum_{\alpha, \beta} A_{\alpha\beta}^* B_{\alpha\beta} = \text{Tr} [A^\dagger B]. \quad (6)$$

It is the complex Euclidean inner product with $|\mathbf{r}_\alpha\rangle \langle \mathbf{r}_\beta|$ s as basis vectors (equivalently, $|u_{p\mathbf{k}}\rangle \langle u_{q\mathbf{k}}|$ s at any fixed \mathbf{k} as basis vectors). This inner product is Hermitian as it satisfies $(B, A)^* = (A, B)$. The Hermitian metric tensor (a.k.a. quantum geometric tensor) in the tangent subspace spanned by

\hat{e}_a^{mn} s is defined by Hilbert-Schmidt inner product of the tangent basis vectors:

$$Q_{ba}^{mn} \equiv (\hat{e}_b^{mn}, \hat{e}_a^{mn}) = r_{nm}^b r_{mn}^a. \quad (7)$$

This metric is identical to the Fubini-Study metric of the state $|u_n\rangle$ in two-band systems, but the two are generally different; the Fubini-Study metric is defined on the whole tangent space of the complex projective space $\mathbb{C}P^{N-1} = U(N)/[U(N-1) \times U(1)]$ (see Methods 10 for details).

The covariant derivative of \hat{e}_a^{mn} s define other geometric quantities such as the connection and curvature. By taking a derivative on \hat{e}_a^{mn} , one obtains parallel and perpendicular components: $\partial_c \hat{e}_a^{mn} = \sum_b C_{ca}^{mn|b} \hat{e}_b^{mn} + \dots$ where the ellipsis indicates the components perpendicular to \hat{e}_a^{mn} s. [Fig. 1]. Then, the covariant derivative ∇ is defined as the parallel-transported part by $\nabla_c \hat{e}_a^{mn} = \sum_b C_{ca}^{mn|b} e_b$. The Hermitian connection is

$$C_{bca}^{mn} \equiv \sum_e Q_{be}^{mn} C_{ca}^{mn|e} = (\hat{e}_b^{mn}, \nabla_c \hat{e}_a^{mn}) = r_{nm}^b r_{mn,c}^a, \quad (8)$$

where $O_{mn,c} \equiv \partial_c O_{mn} - i[\mathcal{A}_c, O]_{mn}$ is called the generalized derivative [28], where $(\mathcal{A}_c)_{mn} = \delta_{mn} \langle u_m | i\partial_c | u_n \rangle$ is the $U(1)^N$ Berry connection. This connection has nontrivial torsion $T_{bca}^{mn} = C_{bca}^{mn} - C_{bac}^{mn}$ in general, which originates from virtual transitions among three states (see Methods 5). Our construction gives a definite geometric meaning to this derivative. One can also take double covariant derivatives to define the second-order connection

$$D_{badc}^{mn} \equiv (\hat{e}_b^{mn}, \nabla_d \nabla_c \hat{e}_a^{mn}) = r_{nm}^b r_{mn,cd}^a, \quad (9)$$

where $r_{mn,cd}^a = (r_{mn,c}^a)_{,d}$. Anti-symmetrizing the two covariant derivatives gives the Hermitian curvature tensor (see Methods 5)

$$K_{badc}^{mn} = D_{badc}^{mn} - D_{bacd}^{mn} = -ir_{nm}^b [\mathcal{F}_{dc}, r^a]_{mn}. \quad (10)$$

Here, $(\mathcal{F}_{dc})_{pq} = \partial_d (\mathcal{A}_c)_{pq} - \partial_c (\mathcal{A}_d)_{pq}$ is the $U(1)^N$ Berry curvature.

Q , C , D , and K defined here are properties of a one-dimensional complex vector space. Their real part define the Riemannian metric tensor (a.k.a quantum metric tensor), metric connection, and the Riemann curvature tensor of the corresponding two-dimensional real vector space spanned by $\text{Re}[\hat{e}_a]$ s and $\text{Im}[\hat{e}_a]$ s. On the other hand, the (minus) imaginary parts define the symplectic form, almost symplectic connection, and the symplectic curvature tensor [32]. All are gauge invariant.

As the geometric quantities defined above are given by the transition dipole moment and its gauge-invariant derivatives, they are basic building blocks of the optical conductivity tensors. The Hermitian metric appears in the linear optical conductivity tensor as

$$\sigma^{b;a} = \frac{\pi \omega e^2}{h} \sum_{m,n} \int_{\mathbf{k}} \delta(\omega - \omega_{mn}) f_{nm} Q_{ba}^{mn}, \quad (11)$$

where $\int_{\mathbf{k}} = \int d^d k / (2\pi)^d$, $\hbar \omega_{mn}$ is the energy difference between m and n bands, and $f_{nm} = f_n - f_m$ is the difference between the Fermi-Dirac distribution of the n and m states.

Also, the Hermitian metric is directly related to the optical transition rate by the Fermi's Golden rule since $|\langle \psi_{mk} | e\hat{\mathbf{r}} \cdot \mathbf{E}(\omega) | \psi_{nk} \rangle|^2 \propto Q_{ba}^{mn} E_b(\omega) E_a^*(\omega)$. This relation is particularly useful for the interpretation of geometric quantities [Fig. 1(c)]. For example, let us consider the injection photovoltaic effect, the photocurrent generation by the optical transition of the electron velocity. The corresponding second-order conductivity tensor can be expressed in terms of the Hermitian metric as

$$\sigma_{\text{inj}}^{c;ab} = \frac{\pi e^3}{\hbar^2 \Gamma} \sum_{m,n} \int_{\mathbf{k}} \delta(\omega - \omega_{mn}) f_{nm} Q_{ba}^{mn} (v_{mm}^c - v_{nn}^c), \quad (12)$$

where v_{mm}^c and v_{nn}^c are the group velocities of bands m and n , respectively, which involve the band dispersion.

To explain the Hermitian connection, we write it as $C_{bca} = r_{nm}^b r_{mn,c}^a = -ir_{nm}^b r_{mn}^a R_{mn}^{c,a}$, where $R_{mn}^{c,a} = \mathcal{A}_{mm}^c - \mathcal{A}_{nn}^c + i\partial_c \log r_{mn}^a$ is the shift vector describing the shift of the electron position during the optical excitation (note that $R_{mn}^{c,a} \sim r_{mm}^c - r_{nn}^c$) [24, 33]. As $r_{nm}^b r_{mn}^a$ is proportional to the transition rate, C_{bca} is responsible for the shift photovoltaic effect, a generation of the direct current $j_{\text{shift}}^c \propto \partial R^c / \partial t$ by illumination of light:

$$\sigma_{\text{shift}}^{c;ab} = \frac{\pi e^3}{2\hbar^2} \sum_{m,n} \int_{\mathbf{k}} \delta(\omega - \omega_{mn}) f_{nm} i(C_{bca}^{mn} - (C_{acb}^{mn})^*). \quad (13)$$

While the above relations generalize the ones found in two-band systems [16–18], the optical manifestation of the Hermitian curvature has not been known even in two-band systems. However, we can also interpret the Hermitian curvature $K_{badc} = -ir_{nm}^b [\mathcal{F}_{dc}, r^a]_{mn} = -ir_{nm}^b r_{mn}^a (\mathcal{F}_{mm}^{dc} - \mathcal{F}_{nn}^{dc})$ in the same vein as the optical transition of the Berry curvature [Fig. 1(c)]. Since the Berry curvature is the source of the Hall effect, the Hermitian curvature is expected to be responsible for the light-induced dc Hall effect, also called the photovoltaic Hall effect [34], which grows linearly in time with constant light intensity. At finite relaxation rate Γ of electronic quasiparticles, the saturated photovoltaic Hall conductivity is proportional to Γ^{-1} ; we call this as the injection photovoltaic Hall conductivity following Ref. [35]. We elaborate more on this response below.

The expression of the third-order injection conductivity tensor in time-reversal-symmetric systems was derived in Ref. [35]. When generalized to include time-reversal-breaking systems, the third-order injection conductivity tensor contains the Hermitian curvature.

$$\sigma_{\text{inj}}^{d;abc} = \frac{\pi e^4}{6\Gamma \hbar^3} \sum_{m,n} \int_{\mathbf{k}} \delta(\omega - \omega_{mn}) f_{nm} i K_{badc}^{mn} + \dots, \quad (14)$$

where the index a is for the static electric field, indices b and c are for the oscillating electric field of light, the ellipsis includes the second-order connection, connection, metric, and virtual transitions among three states (see Methods

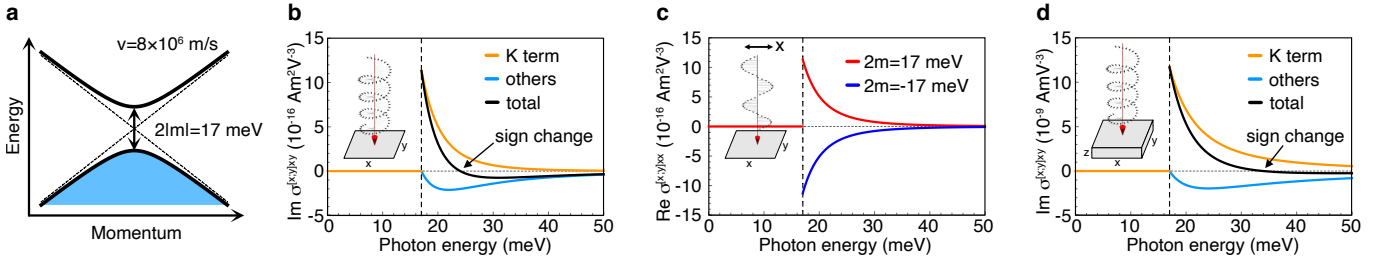


FIG. 2: Third-order photovoltaic Hall conductivity of a Dirac fermion. **a**, Band structure of a massive Dirac fermion. The blue shaded region shows the occupied states. We take the asymptotic velocity $v = 8 \times 10^6$ m/s and the band gap $2|m| = 17$ meV for both 2D and 3D Dirac fermions. **b** and **c**, Two dimensional Dirac fermion. Incident light is circularly polarized in **b** and linearly polarized in **c**. **d**, Three dimensional Dirac fermion. The conductivity of a single Weyl fermion is the half of that in **d**. We take the relaxation rate of $\hbar\Gamma = 1$ meV in all calculations. All non-vanishing tensor components not shown in the figures are related to the shown components by rotational symmetries.

3). The real (imaginary) part of the tensor is responsible for the response independent (dependent) on the light helicity, which we call linear (circular) photoconductivity. The photovoltaic Hall response is characterized by the anti-symmetric part $\sigma_{\text{inj}}^{[d;a]bc} = (\sigma_{\text{inj}}^{d;abc} - \sigma_{\text{inj}}^{a;dbc})/2$. In the clean limit where $\hbar\Gamma$ is much smaller than the photon energy and band gaps, injection response is the largest contribution to the photovoltaic Hall response.

In time-reversal-symmetric systems, the injection response depends on the helicity of the circularly polarized light [Table. 1]. Similarly, spacetime-inversion symmetry also allows only circular photoconductivity because the third-order optical conductivity tensor is invariant under spatial inversion. On the other hand, when time reversal symmetry and spacetime inversion symmetry are both broken, linearly polarized light can also induce injection photovoltaic Hall conductivity.

Equation (14) in general has a complicated form including various geometric quantities. However, as we show now, the Hermitian curvature dominates the photovoltaic Hall response near the band edge of topological materials such as topological insulators and massive Dirac semimetals, characterized by massive Dirac Hamiltonians.

Let us consider the model of a two-dimensional Dirac fermion [Fig. 2(a)].

$$H(\mathbf{k}) = \hbar v(k_x \sigma_x + k_y \sigma_y) + m \sigma_z. \quad (15)$$

As the nonzero mass term break time reversal $T = i\sigma_y K$ and spacetime inversion $PT = \sigma_x K$ symmetries, both linear and circular photovoltaic Hall effects can occur.

We first consider circularly polarized light. Figure 2(b) shows the third-order photovoltaic Hall conductivity tensors calculated with $\hbar\Gamma = 1$ meV, $v = 8 \times 10^5$ m/s, and $2|m| = 17$ meV, which are relevant to graphene on a hexagonal boron nitride substrate [36]. The Hermitian curvature dominates the response near the band edge, while the other contributions having the opposite sign grows as the photon energy goes higher. This leads to the sign change of the third-order conductivity at $2\sqrt{2}|m| = 24$ meV. Since the circular photovoltaic Hall conductivity is T - and PT -symmetric, it is independent of the sign of the mass m .

On the other hand, the linear photovoltaic Hall conductiv-

ity tensor changes sign as the mass sign changes, reflecting the fact that the linear photovoltaic Hall effect is a time-reversal-breaking effect [Fig. 2(c)]. Another feature of the linear photovoltaic Hall conductivity in Fig. 2(c) is that no sign change occurs as the photon energy increases above the band gap. This is because the response is purely from the Hermitian curvature in our model.

Three-dimensional massive Dirac fermions show responses similar to two-dimensional Dirac fermions [Fig. 2(d)]. However, their linear photovoltaic Hall conductivity is zero because of spacetime inversion symmetry. See Methods 8 for analytic expressions of conductivity tensors.

We test our model-based predictions by performing first-principles calculations for monolayer germanene, bulk Bi_2Se_3 , and $(\text{LaOsO}_3)_2$ bilayer [Fig. 3]. These materials are \mathbb{Z}_2 topological insulators in two and three dimensions [37, 38], and a Chern insulator [39], respectively, described by a massive Dirac Hamiltonian close to the band edge. As expected from model calculations, the Hermitian curvature dominates the response near the band edge, and the third-order circular photovoltaic Hall conductivity changes sign as the photon energy increases [Fig. 3(c)]. Ferromagnetic $(\text{LaOsO}_3)_2$ bilayer can additionally show the linear photovoltaic Hall effect because time reversal symmetry is broken [Fig. 3(d)]. Our calculations demonstrate that the Hermitian curvature is a useful measure of the photovoltaic Hall response

Response	Jerk	Injection		Shift	
	Linear	Linear	Circular	Linear	Circular
Photovoltaic Hall effect	No	Yes			
T or PT symmetry	Yes	No	Yes	Yes	No

TABLE 1: Properties of the third-order photoconductivity tensors. Following Ref. [35], the third-order photoconductivity is classified into jerk, injection, and shift according to their dependence on the relaxation rate; they are proportional to Γ^{-2} , Γ^{-1} , and Γ^0 , respectively. Linear (circular) means the light-helicity-independent (-dependent) response. T and P indicate time reversal and spatial inversion. Since third-order optical conductivity tensors are invariant under spatial inversion, time-reversal-symmetric responses are spacetime-inversion-symmetric also.

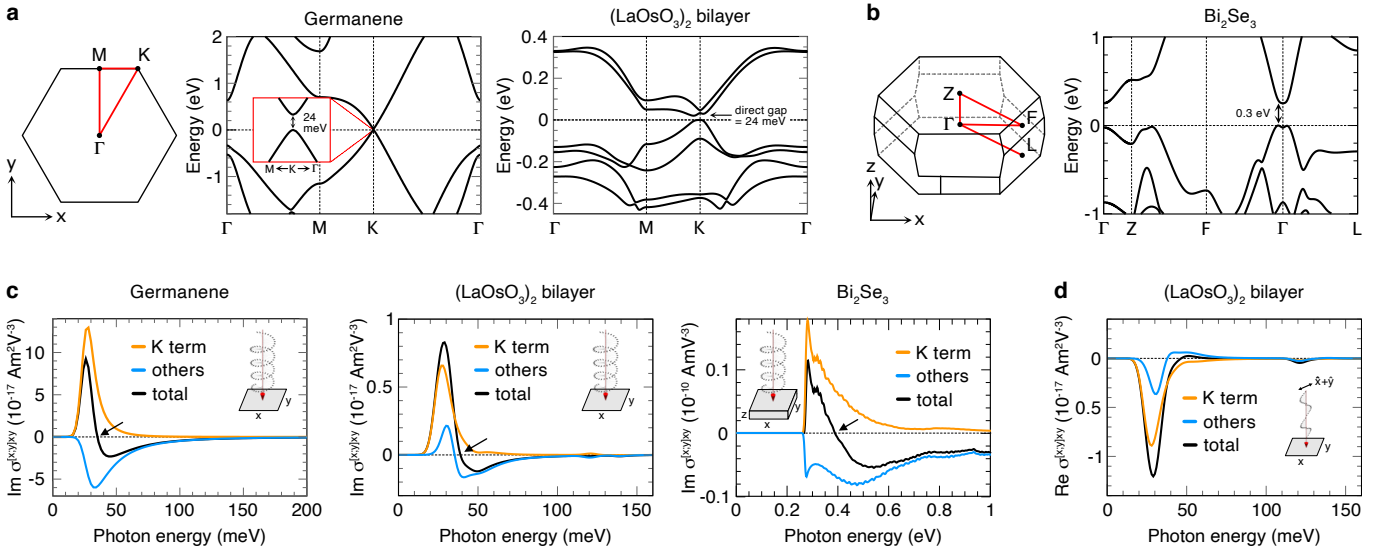


FIG. 3: First-principles calculations on massive Dirac materials. Band structures of (a) monolayer germanene and ferromagnetic (LaOsO₃)₂ bilayer and (b) bulk Bi₂Se₃ along the high-symmetry lines. The top of valence bands is set to 0 eV. **c**, Third-order circular photovoltaic Hall conductivity tensors. Black arrows point to the sign change of the third-order conductivity tensor. **d**, Third-order linear photovoltaic Hall conductivity tensor. Only (LaOsO₃)₂ bilayer shows nonzero response. The Gaussian broadening of 5 meV is introduced to numerically calculate the the delta function. We take the relaxation energy scale to be $\hbar\Gamma = 1$ meV in all cases.

in topological materials.

To conclude, our interpretation of transition dipole moment matrix elements as tangent vectors provides a concrete conceptual ground for studying the geometry of optical transitions. Given an understanding of geometry, one interesting question is about its topology. According to the Gauss-Bonnet theorem associated with the Riemann curvature tensor R^{mn} , the Euler number is related to the first Chern number c_1 of n and m bands by $\chi^{mn} = c_1^n - c_1^m$. Similar topological relations exist in PT -symmetric systems where the first Chern number is trivial (see Methods 9 and Supplementary Note 1). Finding a quantized optical response due to the Euler number χ^{mn} is an intriguing research direction.

Our theoretical approach can be applied beyond optical responses. It allows a systematic understanding of the geometric responses to static electromagnetic fields (see Methods 10) and also other types of responses such as opto-thermal responses, including the photovoltaic thermal Hall and Seebeck effects. Another interesting direction is to study the real-space quantum geometry by identifying momentum operators as tangent vectors. We leave these directions for future studies.

Methods

1. Conventions and Definitions.

- $-e$ is the electron charge. $e > 0$.

- Typical quantities in optical conductivity tensors.

$$\begin{aligned}
 \partial_a &= \frac{\partial}{\partial k_a}, \\
 \int_{\mathbf{k}} &= \int \frac{d^d k}{(2\pi)^d}, \\
 \hat{H}_0 &= \text{single-particle Hamiltonian without external field} \\
 E_n &= \langle \psi_{n\mathbf{k}} | \hat{H}_0 | \psi_{n\mathbf{k}} \rangle = \langle u_{n\mathbf{k}} | \hat{H}_0(\mathbf{k}) | u_{n\mathbf{k}} \rangle, \\
 v_{mn}^a &= \frac{i}{\hbar} \langle \psi_{m\mathbf{k}} | [\hat{r}^a, \hat{H}_0] | \psi_{n\mathbf{k}} \rangle = \hbar^{-1} \langle u_{m\mathbf{k}} | \partial_a \hat{H}_0(\mathbf{k}) | u_{n\mathbf{k}} \rangle, \\
 f_m &= \text{Fermi-Dirac distribution of the } m\text{th band}, \\
 \omega_{mn} &= \hbar^{-1} (E_m - E_n), \\
 f_{mn} &= f_m - f_n, \\
 r_{mn;c}^a &= i\delta_{mn}\partial_a + \langle u_{m\mathbf{k}} | i\partial_a | u_{n\mathbf{k}} \rangle, \\
 (\mathcal{A}_a)_{mn} &= \langle u_{m\mathbf{k}} | i\partial_a | u_{n\mathbf{k}} \rangle \delta_{E_m, E_n} \\
 \mathcal{D}_a &= \partial_a - i\mathcal{A}_a, \\
 r_{mn;c}^a &= [\mathcal{D}_c, r_{mn}^a]_{mn}, \\
 \mathcal{F}_{ba} &= i[\mathcal{D}_b, \mathcal{D}_a] = \partial_b \mathcal{A}_a - \partial_a \mathcal{A}_b - i[\mathcal{A}_b, \mathcal{A}_a]. \quad (16)
 \end{aligned}$$

- Definition of geometric quantities in momentum space defined for a pair of energy levels E_n and E_m . We consider degenerate states $|u_{n_i}\rangle$ s with $E_{n_i} = E_n$ and $|u_{m_j}\rangle$ s with $E_{m_j} = E_m$.

$$\begin{aligned}
Q_{ba} &= \sum_{i,j} r_{n_i m_j}^b r_{m_j n_i}^a \equiv g_{ba} - iF_{ba}/2, \\
C_{abc} &= \sum_{i,j} r_{n_i m_j}^b r_{m_j n_i, c}^a \equiv \Gamma_{bca} - i\tilde{\Gamma}_{bca}, \\
K_{badc} &= \sum_{i,j} r_{n_i m_j}^b r_{m_j n_i, dc}^a - r_{nm}^b r_{mn, cd}^a \equiv R_{badc} - i\tilde{R}_{badc}, \\
D_{badc} &= \sum_{i,j} r_{n_i m_j}^b r_{m_j n_i, dc}^a. \tag{17}
\end{aligned}$$

- Name of geometric quantities

$Q_{ba} = g_{ba} - iF_{ba}/2$	Hermitian metric
g_{ba}	Riemannian metric
$F_{ba}/2$	symplectic form
$C_{bca} = \Gamma_{bca} - i\tilde{\Gamma}_{bca}$	Hermitian connection
Γ_{bca}	metric connection
$\tilde{\Gamma}_{bca}$	symplectic connection
$K_{badc} = R_{badc} - i\tilde{R}_{badc}$	Hermitian curvature
R_{badc}	Riemann curvature tensor
\tilde{R}_{badc}	symplectic curvature tensor
D_{badc}	second-order connection

(18)

2. Nonlinear conductivity tensors. By perturbatively expanding the current expectation value in terms of external electric fields, one obtains

$$j^a(t) = -e \sum_k \sum_{a_1, \dots, a_k} \left[\prod_{i=1}^k \int_{-\infty}^{t_{i+1}} \frac{ie}{\hbar} E^{a_i}(t_i) \right] \langle [\hat{r}^{a_k}, \dots, [\hat{r}^{a_1}, \hat{v}^a]] \rangle, \tag{19}$$

where $t_{k+1} = t$ at each order k . The Fourier components of the k th-order optical conductivity tensors $\tilde{\sigma}^{a;a_1, \dots, a_k}$ are defined by

$$\begin{aligned}
j^a(\Omega) &= \sum_k \sum_{\substack{a_1, \dots, a_k \\ \omega_1, \dots, \omega_k}} E^{a_1}(\omega_1) \dots E^{a_k}(\omega_k) \\
&\times \tilde{\sigma}^{a;a_1, \dots, a_k}(\Omega; \omega_1, \dots, \omega_k) \delta_{\Omega, \sum_{i=1}^k \omega_i}, \tag{20}
\end{aligned}$$

where we Fourier transform the current and electric fields using $f(t) = \sum_{\omega} f(\omega) e^{-i\omega t}$, and the Fourier component satisfies $f(-\omega) = [f(\omega)]^*$ because $f(t)$ we consider is real valued. The conductivity tensor (unsymmetrized) has the form [29]

$$\begin{aligned}
\tilde{\sigma}^{a;a_1, \dots, a_k}(\Omega, \omega_1, \dots, \omega_k) &= -e \left(\frac{ie}{\hbar} \right)^k \\
&\times \int_{\mathbf{k}} \sum_n f_n \langle \psi_{n\mathbf{k}} | [\hat{r}^{a_k}, G_k \circ \dots \circ [\hat{r}^{a_1}, G_1 \circ v^{a_{k+1}}]] | \psi_{n\mathbf{k}} \rangle, \tag{21}
\end{aligned}$$

where f_n is the Fermi-Dirac distribution of the n th band, $\langle \psi_{m\mathbf{k}'} | \hat{r}^a | \psi_{n\mathbf{k}} \rangle = \delta_{mn} i \partial_a \delta_{\mathbf{k}', \mathbf{k}} + \langle u_{m\mathbf{k}'} | i \partial_a | u_{n\mathbf{k}} \rangle$ in momentum space, $A \circ B = \sum_{\alpha, \beta} A_{\alpha\beta} B_{\alpha\beta}$ is the Hadamard product in the Hilbert space, and $G_i = [-i(\hat{\omega} + \sum_{i=1}^k \omega_i)]^{-1}$, where $\langle \psi_{m\mathbf{k}'} | \hat{\omega} | \psi_{n\mathbf{k}} \rangle = \omega_{mn} \delta_{\mathbf{k}', \mathbf{k}}$, and $\omega_{mn} = \hbar^{-1} (E_m - E_n)$. When the first operator \hat{r}^{a_k} acts as a derivative, it produces total derivative terms, which are Fermi surface contributions. The other terms are inter-band contributions.

In this work, we use the symmetrized conductivity tensor defined by [26]

$$\begin{aligned}
\sigma^{a;a_1, \dots, a_k}(\Omega, \omega_1, \dots, \omega_k) \\
= \frac{1}{N_P} \sum_{\text{Perm}} \tilde{\sigma}^{a;a_1, \dots, a_k}(\Omega, \omega_1, \dots, \omega_k), \tag{22}
\end{aligned}$$

where \sum_{Perm} is the summation over all permutations of the k pairs (a_i, ω_i) for $i = 1, \dots, k$, and $N_P = \sum_{\text{Perm}} 1$ is the number of all possible permutations.

3. Photoconductivity tensors. We are interested in the third-order photoconductivity described by

$$j^d(0) = [\sigma_{\text{dark}}^{d;a} + \sigma_{\text{photo}}^{d;a}(\omega)] E^a(0), \tag{23}$$

where $\sigma_{\text{dark}}^{d;a}$ is the linear conductivity without incident light,

$$\sigma_{\text{photo}}^{d;a}(\omega) = 6 \sum_{b,c} \sigma^{d;abc}(0, 0, \omega, -\omega) E^b(\omega) E^c(-\omega) \tag{24}$$

is the photoconductivity, and

$$\begin{aligned}
&\sigma^{d;abc}(0; 0, \omega, -\omega) \\
&= \frac{1}{6} \left[\tilde{\sigma}^{d;abc}(0; 0, \omega, -\omega) + \tilde{\sigma}^{d;acb}(0, 0, -\omega, \omega) \right. \\
&+ \tilde{\sigma}^{d;cab}(0; -\omega, 0, \omega) + \tilde{\sigma}^{d;bac}(0; \omega, 0, -\omega) \\
&\left. + \tilde{\sigma}^{d;bca}(0; \omega, -\omega, 0) + \tilde{\sigma}^{d;cba}(0; -\omega, \omega, 0) \right] \tag{25}
\end{aligned}$$

is the symmetrized third-order photoconductivity tensor. It consists of jerk, injection, and shift responses that are proportional to Γ^{-2} , and Γ^{-1} , and Γ^0 [35]. In the clean limit where the relaxation energy scale $\hbar\Gamma$ is much smaller than the photon energy $\hbar\omega$ and the band gaps $\hbar\omega_{mn}$ s, the jerk response is the most dominant response. However, it does not generate Hall conductivity because $\sigma_{\text{jerk}}^{d;abc}(0; 0, \omega, -\omega) = \frac{\pi e^4}{\hbar^3} \frac{1}{6\Gamma^2} \int_{\mathbf{k}} \sum_{n,m} f_{nm} \delta(-\omega + \omega_{mn}) 2r_{nm}^c r_{mn}^b \partial_a \partial_d \omega_{mn}$ is symmetric with respect to indices a and d . Accordingly, the most dominant photovoltaic Hall conductivity comes from the

injection response.

$$\begin{aligned} \sigma_{\text{inj}}^{d;abc}(0; 0, \omega, -\omega) &= \frac{\pi e^4}{\hbar^3} \frac{1}{6\Gamma} \int_{\mathbf{k}} \sum_{n,m} f_{nm} \delta(-\omega + \omega_{mn}) \times \\ &i \left\{ K_{cbad}^{mn} + D_{cb(ad)}^{mn} - (D_{bc(ad)}^{mn})^* \right. \\ &+ \sum_e \left((C_{edc}^{mn})^* C_{ab}^{mn|e} - (C_{eac}^{mn})^* C_{db}^{mn|e} \right) \\ &+ 2 \frac{\partial_d \omega_{mn}}{\omega_{mn}} [C_{cba}^{mn} - (C_{bca}^{mn})^*] \\ &- 2 \frac{\partial_d \omega_{mn}}{\omega_{mn}} \left(Q_{ca}^{mn} \frac{\partial_b \omega_{mn}}{\omega_{mn}} - (Q_{ba}^{mn})^* \frac{\partial_c \omega_{mn}}{\omega_{mn}} \right) \\ &+ 2 \partial_d \omega_{mn} \sum_{p: E_p \neq E_m, E_n} \left[r_{nm}^c \left(r_{mp}^b \frac{r_{pn}^a}{\omega_{pn}} - \frac{r_{mp}^a}{\omega_{mp}} r_{pn}^b \right) \right. \\ &\left. \left. + \left(r_{np}^c \frac{r_{pm}^a}{\omega_{pm}} - \frac{r_{np}^a}{\omega_{np}} r_{pm}^c \right) r_{mn}^b \right] \right\}, \end{aligned} \quad (26)$$

where $K_{cbad}^{mn} = r_{nm}^c (r_{mn,da}^b - r_{mn,ad}^b)$, $D_{cb(ad)}^{mn} = \frac{1}{2} r_{nm}^c (r_{mn,da}^b + r_{mn,ad}^b)$, $Q_{ba}^{mn} = r_{nm}^b r_{mn}^a$, $\sum_e Q_{ce}^{mn} C_{ba}^{mn|e} = C_{cba}^{mn} = r_{nm}^c r_{mn}^a$, $\sum_e (C_{edc}^{mn})^* C_{ab}^{mn|e} = r_{nm,d}^c r_{mn,a}^b$, $O_{mn,a} = \partial_a O_{mn} - i[\mathcal{A}, O]_{mn}$, and $\mathcal{A}_{mn} = \delta_{E_m, E_n} \langle u_m | \partial_a | u_n \rangle$ is the Berry connection. $\delta_{E_m, E_n} = \delta_{mn}$ when bands are all non-degenerate, as we assume in the most of part of the main text.

4. Maurer-Cartan form. Here we explain the basic concept of the Maurer-Cartan form (See Ref. [40] for further information). Let us consider the space of complex $N \times N$ matrices $M(N, \mathbb{C})$, defining an N^2 -dimensional complex Euclidean space \mathbb{C}^{N^2} . The geometrical structure of subspaces such as $U(N)$ or $U(N)/U(1)^N$ is induced from the structure of $M(N, \mathbb{C})$. Given a matrix representation, we can define Euclidean coordinates x^{ij} with $i, j = 1, \dots, N$ by

$$x^{ij}(g) = g^{ij}, \quad g \in M(N, \mathbb{C}), \quad (27)$$

where g^{ij} is the matrix element of g . The tangent space at g is spanned by $\frac{\partial}{\partial x^{ij}}|_g$. Here the symbol $|_g$ indicate that it is defined at the point $g \in M(N, \mathbb{C})$. Two tangent basis vectors $\frac{\partial}{\partial x^{ij}}|_g$ and $\frac{\partial}{\partial x^{ij}}|_{g'}$ are different objects when $g \neq g'$ because they live at distinct points.

Let us restrict our attention to the space of invertible matrices $GL(N, \mathbb{C})$. The left multiplication $L_f : g \rightarrow fg$ for invertible matrices f and g induces a push-forward mapping L_{f*} between their tangent vectors

$$L_{f*} \partial_{x^{ij}}|_g = \frac{\partial x^{kl}(fg)}{\partial x^{ij}(g)} \partial_{x^{kl}}|_{fg} \quad (28)$$

Using the property of the coordinates we choose in equation (27), we have

$$L_{f*} X|_g = \sum_{k,j} [f X(g)]^{kj} \partial_{x^{kj}}(fg) \quad (29)$$

for any vector field X , where $X|_g = \sum_{i,j} X^{ij}(g) \partial_{x^{ij}}(g)$ is a tangent vector at g defined by X , and $(fX)^{kl} = \sum_m f^{km} X^{ml}$ is the matrix product. If we take $f = g^{-1}$ and consider the vector field describing the tangent basis vectors obtained by momentum space coordinates k^a 's, i.e., $X(g) = \partial_a|_g = \sum_{ij} [\partial_a x^{ij}(g)] \partial_{x^{ij}}(g)$,

$$L_{g^{-1}*} \left[\sum_{i,j} (\partial_a g^{ij}) \partial_{x^{ij}}(g) \right] = \sum_{k,j} (g^{-1} \partial_a g)^{kj} \partial_{x^{kj}}(1), \quad (30)$$

where 1 is the identity matrix. This shows that the Maurer-Cartan form $\xi_a = g^{-1} \partial_a g$ is the tangent vector at g that is sent back to the Lie algebra $gl(N, \mathbb{C})$, which is the tangent space defined at the identity matrix. More formally, as a differential form, the Maurer-Cartan form is defined as a linear map from tangent vectors to the Lie algebra by $\xi(X|_g) \equiv L_{g^{-1}*} X|_g$, from which $\xi(\partial_a|_g) = g^{-1} \partial_a g$. We simply call the Lie algebras $g^{-1} \partial_a g$ s Maurer-Cartan forms as is typical.

The Lie bracket of two tangent vector fields $L_{g^{-1}*} X$ and $L_{g^{-1}*} Y$ can be evaluated from the Lie bracket of X and Y by $[L_{g^{-1}*} X, L_{g^{-1}*} Y]_{\text{LB}} = L_{g^{-1}*} [X, Y]_{\text{LB}}$. Since $[X, Y]_{\text{LB}} = 0$ for coordinate vectors $X(g) = \partial_a|_g$ and $Y(g) = \partial_b|_g$, we have $[g^{-1} \partial_a g, g^{-1} \partial_b g]_{\text{LB}} = 0$.

5. Riemannian geometry with degenerate states. Let us consider two distinct energy levels E_n and E_m with N_d - and M_d -fold degenerate states $|u_{n_i}\rangle$ and $|u_{m_j}\rangle$, respectively, where $i = 1, \dots, N_d$ and $j = 1, \dots, M_d$. Then, the tangent vector associated with the momentum coordinate k^a is defined by

$$\hat{e}_a^{mn} \equiv \sum_{i,j} r_{m_j n_i}^a |u_{m_j}\rangle \langle u_{n_i}|. \quad (31)$$

The Hermitian metric is evaluated from the Hilbert-Schmidt inner product of two such basis vectors.

$$\begin{aligned} Q_{ba}^{mn} &\equiv (\hat{e}_b^{mn}, \hat{e}_a^{mn}) \\ &= \sum_{ij} r_{n_i m_j}^b r_{m_j n_i}^a. \end{aligned} \quad (32)$$

The covariant derivative is obtained by projecting to the basis $|u_{m_j}\rangle \langle u_{n_i}|$ s after taking an ordinary derivative.

$$\nabla_c \hat{e}_a^{mn} \equiv P_m (\partial_c \hat{e}_a) P_n = \sum_{i,j} r_{m_j n_i, c}^a |u_{m_j}\rangle \langle n_i|, \quad (33)$$

where $P_m = \sum_j |u_{m_j}\rangle \langle u_{m_j}|$, $P_n = \sum_i |u_{n_i}\rangle \langle u_{n_i}|$, and

$$r_{m_j n_i, c}^a = [\mathcal{D}_c, r^a]_{m_j n_i}, \quad (34)$$

where $[A, B] = AB - BA$ is the commutator, $\mathcal{D}_c = \partial_c - i\mathcal{A}^c$, and $\mathcal{A}_{pq} = \delta_{E_p, E_q} \langle u_p | \partial_c | u_q \rangle$ is the $U(N_d) \times U(M_d)$ Berry connection [$U(N_d)$ for n and $U(M_d)$ for m , and forget about the gauge group of the other states here]. The Hermitian connection is then defined by

$$C_{bca}^{mn} \equiv (\hat{e}_b^{mn}, \nabla_c \hat{e}_a^{mn}) = \sum_{ij} r_{n_i m_j}^b r_{m_j n_i, c}^a, \quad (35)$$

It preserves the Hermiticity $(O_{mn,c})^* = O_{nm,c}$ for a Hermitian operator O . Also, this connection satisfies the metric compatibility $\nabla_c(\hat{e}_b^{mn}, \hat{e}_a^{mn}) = (\hat{e}_b^{mn}, \nabla_c \hat{e}_a^{mn}) + (\nabla_c \hat{e}_b^{mn}, \hat{e}_a^{mn})$ because $(\hat{e}_b^{mn}, \nabla_c \hat{e}_a^{mn}) = (\hat{e}_b^{mn}, \partial_c \hat{e}_a^{mn})$, and ∇_c acts as an ordinary derivative on scalars.

The Hermitian connection we define has a non-zero torsion in general when the number of bands exceeds two. The torsion tensor is given by virtual transitions among three bands.

$$\begin{aligned} T_{bca}^{mn} &\equiv (\hat{e}_b^{mn}, \nabla_c \hat{e}_a^{mn} - \nabla_a \hat{e}_c^{mn} - [\hat{e}_c^{mn}, \hat{e}_a^{mn}]) \\ &= C_{bca}^{mn} - C_{bac}^{mn} \\ &= i \sum_{i,j} r_{n_i m_j}^b \sum_{p: E_p \neq E_m, E_n} (r_{m_j p}^c r_{p n_i}^a - r_{m_j p}^a r_{p n_i}^c), \end{aligned} \quad (36)$$

where we use that $[\hat{e}_c^{mn}, \hat{e}_a^{mn}] = 0$.

The Hermitian curvature tensor is defined by

$$K_{badc}^{mn} \equiv (\hat{e}_b^{mn}, (\nabla_d \nabla_c - \nabla_c \nabla_d - \nabla_{[\hat{e}_d^{mn}, \hat{e}_c^{mn}]} \hat{e}_a^{mn})). \quad (37)$$

It is identical to $D_{badc}^{mn} - D_{badc}^{mn}$ because $[\hat{e}_d^{mn}, \hat{e}_c^{mn}] = 0$, where

$$D_{badc}^{mn} \equiv (\hat{e}_b^{mn}, \nabla_d \nabla_c \hat{e}_a^{mn}) = \sum_{ij}^N r_{n_i m_j}^b r_{m_j n_i, cd}^a \quad (38)$$

is the second-order connection, and

$$r_{m_j n_i, cd}^a = [\mathcal{D}_d, [\mathcal{D}_c, r^a]]_{m_j n_i} \quad (39)$$

is the double covariant derivative. The index c of the double covariant derivative does not transform tensorially under general coordinate transformations, in contrast to case of the second covariant derivative $S_{badc}^{mn} = (\hat{e}_b^{mn}, (\nabla_d \nabla_c - \nabla_{\nabla_d \hat{e}_c^{mn}}) \hat{e}_a^{mn})$. However, the double covariant derivative is more convenient for our purpose. The Hermitian curvature tensor can be written as

$$K_{badc}^{mn} = -i \sum_{i,j} r_{n_i m_j}^b [\mathcal{F}_{dc}, r^a]_{m_j n_i}, \quad (40)$$

where \mathcal{F}_{dc} is the Berry curvature $(\mathcal{F}_{dc})_{pq} = i[\mathcal{D}_d, \mathcal{D}_c]_{pq} = (\partial_d \mathcal{A}_c - \partial_c \mathcal{A}_d - i[\mathcal{A}_d, \mathcal{A}_c])_{pq}$. It follows from

$$r_{m_j n_i, cd}^a - r_{m_j n_i, dc}^a = -i[\mathcal{F}_{dc}, r^a]_{m_j n_i}, \quad (41)$$

where we use $[\mathcal{D}_d, [\mathcal{D}_c, r^a]]_{m_j n_i} - [\mathcal{D}_c, [\mathcal{D}_d, r^a]]_{m_j n_i} = [[\mathcal{D}_d, \mathcal{D}_c], r^a]_{m_j n_i}$. A useful property of the Hermitian curvature is

$$(K_{badc}^{mn})^* = K_{abdc}^{mn} \quad (42)$$

which can be shown from equation (40) and the Hermitian property $(K_{badc}^{mn})^* = K_{badc}^{mn}$.

6. Symmetry constraints on the geometric quantities. To study symmetry properties, it is convenient to write \hat{e}_a^{mn} using projection operators as $\hat{e}_a^{mn}(\mathbf{k}) = P_m(\mathbf{k})i\partial_{k_a}P_n(\mathbf{k})$, where

$P_n(\mathbf{k}) = \sum_{i=1}^{N_d} |u_{n_i \mathbf{k}}\rangle \langle u_{n_i \mathbf{k}}|$ is the projection to N_d -fold degenerate states with $E_{n_i} = E_n$.

Let us first consider time reversal symmetry. It imposes $TP_m(\mathbf{k})T^{-1} = P_m(-\mathbf{k})$, where T is the time reversal operator acting on the cell-periodic Bloch states. Accordingly, e_a follows the corresponding symmetry constraint. $T\hat{e}_a^{mn}(\mathbf{k})T^{-1} = P_m(-\mathbf{k})i\partial_{-k_a}[P_n(-\mathbf{k})] = \hat{e}_a^{mn}(-\mathbf{k})$. Using this, one can show that time reversal symmetry imposes

$$G(\mathbf{k}) = G^*(-\mathbf{k}) \quad (43)$$

for $G = Q^{mn}, C^{mn}, D^{mn}$, or K^{mn} .

Spatial symmetry under $g : \mathbf{r} \rightarrow R_g \mathbf{r} + \mathbf{a}_g$ imposes $U_g P_m(\mathbf{k}) U_g^{-1} = P_m(R_g \mathbf{k})$, where U_g is the unitary representation of g for cell-periodic Bloch states. The g symmetry constraint on the tangent vector is $U_g \hat{e}_a^{mn}(\mathbf{k}) U_g^{-1} = P_m(R_g \mathbf{k})i\partial_{k_a}[P_n(R_g \mathbf{k})] = \sum_b (R_g)_{ba} \hat{e}_b^{mn}(-\mathbf{k})$. Geometric quantities then satisfy

$$G_{a_1 \dots a_k}(\mathbf{k}) = (R_g)_{b_1 a_1} \dots (R_g)_{b_k a_k} G_{b_1 \dots b_k}(R_g \mathbf{k}) \quad (44)$$

for $G = Q^{mn}, C^{mn}, D^{mn}$, or K^{mn} .

Spacetime inversion PT symmetry plays a distinguished role because it gives constraints at each \mathbf{k} point. The constraint $PT\hat{e}_a^{mn}(\mathbf{k})(PT)^{-1} = \hat{e}_a^{mn}(\mathbf{k})$ gives a real structure when $(PT)^2 = 1$. This is most clearly seen by taking a gauge where PT is represented by a complex conjugation K , such that $(\hat{e}_a^{mn})^* = \hat{e}_a^{mn}$ is real-valued. It forms a one-dimensional real subspace of the tangent space of the manifold $O(N)/O(1)^N$ of non-degenerate PT -symmetric cell-periodic Bloch states. On the other hand, PT symmetry gives a quaternion structure when $(PT)^2 = -1$. To see this, let us write down the matrix element of \hat{e}_a^{mn} . Each band becomes twofold degenerate by the PT symmetry satisfying $(PT)^2 = -1$ (Kramers theorem). We can fix the gauge such that PT is represented by $i\sigma_y K$ within each set of twofold degenerate states. Then PT symmetry $(r^a)_{m_i n_j}^* = -(i\sigma_y^{-1} r^a i\sigma_y)_{m_i n_j}$ requires that $(r_{m_i n_j}^a) = -i(f_1^a \sigma_0 + f_2^a i\sigma_x + f_3^a i\sigma_y + f_4^a i\sigma_z)$, where σ_0 is the 2×2 identity matrix, and $\sigma_{i=x,y,z}$ are Pauli matrices, and $f_{i=1,2,3,4}^a$ are real-valued functions. The matrices $\{\sigma_0, i\sigma_x, i\sigma_y, i\sigma_z\}$ satisfy the quaternion algebra, defining a quaternionic subspace of the tangent space of the manifold $Sp(N)/Sp(1)^N$ of Kramers degenerate PT -symmetric cell-periodic Bloch states. Independent of the sign of $(PT)^2$, the geometric quantities satisfy $G(\mathbf{k}) = G^*(\mathbf{k})$ for $G = Q^{mn}, C^{mn}, D^{mn}$, or K^{mn} .

7. Riemann curvature tensor of two-level systems. Let us consider a model with two energy levels E_n and E_m which are N_d - and M_d -fold degenerate, respectively. Using that

$$(\mathcal{Q}_{ba}^n)_{n_i n_k} = \sum_{j=1}^{M_d} r_{n_i m_j}^b r_{m_j n_k}^a \quad (45)$$

defines the non-abelian Hermitian metric of the level n (similarly for the level m), where $E_{n_i} = E_{n_k} = E_n$ and $E_{m_j} =$

E_m , we obtain

$$K_{badc}^{mn} = i\text{Tr}_n \mathcal{Q}_{ba}^n \mathcal{F}_{dc}^n - i\text{Tr}_m \mathcal{F}_{dc}^m \mathcal{Q}_{ab}^m, \quad (46)$$

where $\mathcal{Q}_{ba}^n = \mathcal{G}_{ba}^n - (i/2)\mathcal{F}_{ba}^n$ is the non-abelian Hermitian metric of the level E_n , and Tr_n is the trace within the energy level E_n . The non-abelian Riemannian metric \mathcal{G}_{ba}^n and the Berry curvature \mathcal{F}_{ba}^n are respectively symmetric and anti-symmetric with respect to the exchange of a and b .

Now we suppose that the system has chiral S symmetry $SH(\mathbf{k})S^{-1} = -H(\mathbf{k})$ or particle-hole-times-inversion CP symmetry $CPH(\mathbf{k})(CP)^{-1} = -H^*(\mathbf{k})$. Those symmetries impose

$$\begin{aligned} \mathcal{Q}_{ba}^m(\mathbf{k}) &= U_S^{-1} \mathcal{G}_{ba}^n(\mathbf{k}) U_S, \\ \mathcal{Q}_{ba}^m(\mathbf{k}) &= U_{CP}^{-1} [\mathcal{Q}_{ba}^n(\mathbf{k})]^* U_{CP}. \end{aligned} \quad (47)$$

The expression of the Hermitian curvature tensor then reduces to,

$$K_{badc}^{mn} = 2i\text{Tr}_n \mathcal{Q}_{ba}^n \mathcal{F}_{dc}^n. \quad (48)$$

This formula can be applied to the linearized model of Dirac or Weyl point whether it is massive or massless, because such a model has CP or chiral symmetry. One interesting special case is $\text{Re}K_{bab}^{mn} = R_{bab}^{mn} = \text{Tr}_n \mathcal{F}_{ba}^n \mathcal{F}_{ba}^n$, which measures the norm of the non-abelian Berry curvature matrix \mathcal{F}_{ba}^n .

8. Third-order photovoltaic Hall conductivity of Dirac and Weyl fermions. Let us consider a two-dimensional Dirac fermion described by equation (15). The Riemann curvature term is

$$\text{Im}\sigma_K^{[x;y]xy} = \frac{e^4}{12\hbar^3} \frac{1}{\Gamma} \frac{1}{\omega} \left(\frac{v}{\omega}\right)^2 \left(\frac{2m}{\hbar\omega}\right)^2 \Theta(|\omega| - 2|m|), \quad (49)$$

while the remaining term has the opposite sign

$$\begin{aligned} \text{Im}\sigma^{[x;y]xy} - \text{Im}\sigma_K^{[x;y]xy} \\ = -\frac{e^4}{12\hbar^3} \frac{1}{\Gamma} \frac{1}{\omega} \left(\frac{v}{\omega}\right)^2 \left[1 - \left(\frac{2m}{\hbar\omega}\right)^2\right] \Theta(|\omega| - 2|m|). \end{aligned} \quad (50)$$

The Riemann curvature leads to the dominant photovoltaic Hall response near the band edge $\hbar|\omega| = 2|m|$. Other contributions become dominant when $\hbar|\omega| > 2\sqrt{2}|m|$, where the third-order conductivity changes sign. When we take parameters used in the main text, $v = 8 \times 10^6$ m/s and $2|m| = 17$ meV, the peak value $1.2 \times 10^{-15} \text{ Am}^2 \text{ V}^{-2}$ at the band edge. It corresponds to the photoconductivity $\sigma_{\text{photo}}^{x;y} = (e^2/h) \times 3.5 \times 10^{-4} I_{\text{light}}/(1 \text{ W cm}^{-2})$, where $e^2/h = 3.874 \times 10^{-5} \Omega^{-1}$ is the conductance quantum per spin. This magnitude is the same as the photoconductivity for a massless Dirac fermion at $\hbar\omega = 17$ meV, but the sign is opposite.

Nonzero components of the linear photovoltaic Hall conductivity tensor in two dimensions are

$$\begin{aligned} \text{Re}\sigma^{[x;y]yy} &= \text{Re}\sigma^{[x;y]xx} \\ &= \frac{e^4}{24\hbar^3} \frac{1}{\Gamma} \frac{1}{\omega} \left(\frac{v}{\omega}\right)^2 \left(\frac{2m}{\hbar\omega}\right) \left[1 + \left(\frac{2m}{\hbar\omega}\right)^2\right] \Theta(|\omega| - 2|m|), \end{aligned} \quad (51)$$

while $\sigma^{[x;y]xy} = \sigma^{[x;y]yx} = 0$ by rotational symmetry. It is purely by the symplectic curvature tensor.

For a Weyl fermion in three dimensions described by

$$H_{\text{Weyl}} = \hbar v(k_x\sigma_x + k_y\sigma_y + k_z\sigma_z), \quad (52)$$

there is only one non-vanishing linearly independent component of the photovoltaic Hall conductivity tensor, which is

$$\text{Im}\sigma^{[x;y]xy} = -\frac{e^4}{72\pi\hbar^3} \frac{1}{\Gamma} \frac{1}{\omega} \left(\frac{v}{\omega}\right), \quad (53)$$

and $\text{Im}\sigma_K^{[x;y]xy} = -\text{Im}\sigma^{[x;y]xy}$. Other non-zero components are related by $SO(3)$ rotational symmetries

$$\text{Im}\sigma^{[x;y]xy} = \text{Im}\sigma^{[yz];yz} = \text{Im}\sigma^{[zx];zx} \quad (54)$$

and the inherent relations $\text{Im}\sigma^{[a;d]cb} = -\text{Im}\sigma^{[d;a]cb} = -\text{Im}\sigma^{[a;d]bc}$ by definition. The linear photovoltaic Hall conductivity is zero is due to time reversal $T = i\sigma_y K$ symmetry of a Weyl fermion around the crossing point.

Massless Dirac fermions in three dimensions have the photovoltaic Hall conductivity tensors twice that of a Weyl fermion, as it consists of two copies of Weyl fermions. When the mass gap $2m$ is introduced by

$$H_{\text{Dirac}} = \hbar v(k_x\tau_z\sigma_x + k_y\tau_z\sigma_y + k_z\tau_z\sigma_z) + m\tau_x, \quad (55)$$

the non-vanishing linearly independent photovoltaic Hall conductivity component is

$$\text{Im}\sigma^{[x;y]xy} = \frac{e^4}{36\pi\hbar^3} \frac{1}{\Gamma} \frac{1}{\omega} \left(\frac{v}{\omega}\right) \left[4 \left(\frac{2m}{\hbar\omega}\right)^2 - 1\right] \Theta(|\omega| - 2|m|), \quad (56)$$

and

$$\text{Im}\sigma_K^{[x;y]xy} = \frac{e^4}{36\pi\hbar^3} \frac{1}{\Gamma} \frac{1}{\omega} \left(\frac{v}{\omega}\right) \left[1 + 2 \left(\frac{2m}{\hbar\omega}\right)^2\right] \Theta(|\omega| - 2|m|). \quad (57)$$

Here, we use $R_{yxyx}^{cv} = \text{Tr}[(\mathcal{F}_{xy}^n)^2] = 8(v/\omega_{cv})^4[(2\hbar v k_z)^2 + (2m)^2]/(\hbar\omega_{cv})^2$ (c and v indicating the upper- and lower-energy states). See Methods 8. Since the mass preserves $PT = i\tau_x\sigma_y K$, the linear photovoltaic Hall conductivity is zero. It does not depend on the choice of the matrix representation. Any Dirac mass term preserves PT symmetry.

9. Topology of the transition matrix dipole moment. When the spatial dimension d is even, the Euler number is given by the generalized Gauss-Bonnet theorem [2]

$$\chi^{mn} = \int \wedge^d dk \sqrt{g} \sum_{a_i, b_j} \frac{\epsilon^{a_1 a_2 \dots a_{d-1} a_d} \epsilon^{b_1 b_2 \dots b_{d-1} b_d}}{(2\pi)^{d/2} 2^d (d/2)! g} \times R_{a_1 a_2 b_1 b_2}^{mn} \dots R_{a_{d-1} a_d b_{d-1} b_d}^{mn}, \quad (58)$$

where $g \equiv \det g^{mn}$ is the determinant of the metric g^{mn} with respect to its momentum indices that are implicit in this notation, $\wedge^d dk$ is the oriented integral measure, and $R_{a_1 a_2 b_1 b_2}^{mn} = \text{Re} K_{a_1 a_2 b_1 b_2}^{mn}$ is the Riemann curvature tensor.

In two-dimensions, we have

$$\begin{aligned} \chi^{mn} &= \frac{1}{2\pi} \int dk_1 dk_2 \text{sgn}(F_{xy}^{mn}) \frac{R_{xyxy}^{mn}}{\sqrt{g}} \\ &= \frac{1}{2\pi} \int dk_1 dk_2 \frac{|F_{xy}^{mn}| (\mathcal{F}_{xy}^n - \mathcal{F}_{xy}^m)}{2\sqrt{g}} \\ &= \frac{1}{2\pi} \int dk_1 dk_2 (\mathcal{F}_{xy}^n - \mathcal{F}_{xy}^m) \\ &= c_1^n - c_1^m, \end{aligned} \quad (59)$$

where we use $|F_{xy}^{mn}|/2 = g$ following from $\det Q^{mn} = Q_{xx}^{mn} Q_{yy}^{mn} - Q_{xy}^{mn} Q_{yx}^{mn} = 0$. Here, $F_{xy}^{mn} \equiv -2\text{Im}Q_{xy}^{mn}$ should be distinguished from the Berry curvature \mathcal{F} (except in two-band systems). $\det Q^{mn} = 0$ because we introduce two momentum coordinates while Q^{mn} is defined on one-dimensional tangent space (cf. $\det g$ is nonzero because the target space is two-dimensional as a real space). Here, the sign $\text{sgn}(F_{xy}^{mn})$ due to the oriented nature of the integral measure should not be discarded. Without this factor, one obtains a non-quantized value as in Refs. [42–45]

In spin-orbit coupled PT -symmetric systems, where $(PT)^2 = -1$, the transition dipole moments $\hat{e}_a^{m_i n_j}$'s between two pairs of Kramers-degenerate states $|u_{m_{i=1,2}}\rangle$ and $|u_{n_{j=1,2}}\rangle$ with $E_{m_1} = E_{m_2} \neq E_{n_1} = E_{n_2}$ define four-dimensional tangent subspace. Therefore, the Gauss-Bonnet theorem can be applied in a four-dimensional momentum space. The result is

$$\begin{aligned} \chi^{mn} &= \int dk_1 dk_2 dk_3 dk_4 \sum_{a_i, b_j} \frac{\text{sgn}(\wedge^4 k)}{(2\pi)^2 2^4 2\sqrt{g}} \epsilon^{a_1 a_2 a_3 a_4} \epsilon^{b_1 b_2 b_3 b_4} \\ &\quad \times R_{a_1 a_2 b_1 b_2}^{nm} R_{a_3 a_4 b_1 b_4}^{nm} \\ &= \int \frac{d^4 k}{32\pi^2} \sum_{b_j} \epsilon^{b_1 b_2 b_3 b_4} \sum_{i=1}^2 \\ &\quad \times [(\mathcal{F}_{b_1 b_2} \mathcal{F}_{b_3 b_4})_{n_i n_i} - (\mathcal{F}_{b_1 b_2} \mathcal{F}_{b_3 b_4})_{m_i m_i}] \\ &= p_1^n - p_1^m, \end{aligned} \quad (60)$$

where p_1 is the first Pontryagin number. See Supplementary Note 2 for a derivation.

In spinless PT -symmetric systems, where $(PT)^2 = 1$, \hat{e}_a^{mn} define a one-dimensional real tangent vector. Since it is odd-dimensional, the generalized Gauss-Bonnet theorem does not apply. Instead, we can define the first Stiefel-Whitney

number associated with it by

$$w_1^{mn} = \frac{1}{\pi} \oint dk \cdot i\partial_k \log r_{mn}^a \mod 2. \quad (61)$$

It measures the orientability of the tangent vector \hat{e}_a^{mn} over the one-dimensional momentum space. $w_1^{mn} = 0$ ($w_1^{mn} = 1$) indicates that \hat{e}_a^{mn} is orientable (non-orientable). As we show in Supplementary Note 3,

$$w_1^{mn} = w_1^n - w_1^m, \quad (62)$$

where w_1^n and w_1^m are the first Stiefel-Whitney numbers of bands n and m , or equivalently, the Berry phases of bands n and m divided by π [3, 4].

10. Geometry of a single state and others. A single state $|u_n\rangle$ lives on the complex projective manifold

$$\mathbb{C}P^{N-1} = \frac{\text{U}(N)}{\text{U}(1) \times \text{U}(N-1)}, \quad (63)$$

where N is the number of all bands, $\text{U}(N)$ described the degrees of freedom of the cell-periodic Bloch state $U_{\alpha n} = \langle \mathbf{r}_\alpha | u_n \rangle$, $\text{U}(1)$ is the phase rotation of the state $|u_n\rangle$, and $\text{U}(N-1)$ is the unitary transformation of the other states. The tangent vectors on this manifold is described by the Maurer-Cartan form

$$\begin{aligned} \hat{\xi}_a^n &= U^{-1} i\partial_a U - U^{-1} i\partial_a U|_{\text{U}(1)} - U^{-1} i\partial_a U|_{\text{U}(N-1)} \\ &\equiv \hat{e}_a^n + (\hat{e}^n)_a^\dagger, \end{aligned} \quad (64)$$

where $U^{-1} i\partial_a U = \sum_{m,n} |u_m\rangle r_{mn}^a \langle u_n|$ is the Maurer-Cartan form of $\text{U}(N)$, $U^{-1} i\partial_a U|_{\text{U}(1)} = |u_n\rangle \langle u_n| i\partial_a |u_n\rangle \langle u_n|$ is its projection to the $\text{U}(1)$ direction, $U^{-1} i\partial_a U|_{\text{U}(N-1)} = \sum_{m \neq n, p \neq n} |u_m\rangle \langle u_m| i\partial_a |u_p\rangle \langle u_p|$ is the projection to $\text{U}(N-1)$ direction, and

$$\hat{e}_a^n = \sum_{m: m \neq n} |u_m\rangle r_{mn}^a \langle u_n|. \quad (65)$$

The Hermitian metric tensor of the n th band is

$$Q_{ba}^n = (\hat{e}_b^n, \hat{e}_a^n) = \sum_{m: m \neq n} r_{nm}^b r_{mn}^a. \quad (66)$$

This is the Fubini-Study metric. Equivalently, it can be defined by $Q_{ba}^n = \frac{1}{2} [(\hat{\xi}_b, \hat{\xi}_a) - i(\hat{\xi}_b, i\hat{\xi}_a)]$. In two-band systems, the Fubini-Study metric is identical to the metric in equation (7) because there is only one pair of bands (m, n) ; this is the reason why the geometric understanding of optical responses in two-band systems was possible through the Fubini-Study metric in the previous works [16–18]. The imaginary part of the Fubini-Study metric, the symplectic form, is identical to the Berry curvature of the band n . The Hermitian connection, torsion, and curvature can be defined from the covariant derivative

$$O_{mn,c} = \left[\partial_c - i\mathcal{A}_c^{\text{U}(1)} - i\mathcal{A}_c^{\text{U}(N-1)}, O \right]_{mn}, \quad (67)$$

where $(\mathcal{A}_c^{\text{U}(1)})_{mp} = \delta_{mn}\delta_{pn} \langle u_n | i\partial_c | u_n \rangle$ is the $\text{U}(1)$ Berry connection of band n , $(\mathcal{A}_c^{\text{U}(N-1)})_{mp} = (1 - \delta_{mn})(1 - \delta_{pn}) \langle u_m | i\partial_c | u_p \rangle$ is the $\text{U}(N-1)$ Berry connection of the other bands.

Note that the torsion tensor is zero because $r_{mn,c}^a - r_{mn,a}^c = \partial_c r_{mn}^a - \partial_a r_{mn}^c - i[r^c, r^a]_{mn} = 0$. It is due to the fact that we consider the tangent space of a Kähler manifold, which has zero torsion [40]. Any of its complex submanifolds also has zero torsion because it is a Kähler manifold [40]. Let us compare this with that \hat{e}_a^{mn} defines a subspace of the tangent space of the projective space. The non-zero torsion (see Methods 5) of our connection for \hat{e}_a^{mn} is the manifestation that the subspace of a tangent space may not define a tangent space of a submanifold by a topological obstruction (see Supplementary Note 1), i.e., not every vector bundle of dimension D defines a tangent bundle of dimension D . The torsionless connection is called the Levi-Civita connection.

The manifold of the whole occupied states is described by the complex Grassmannian manifold

$$\text{Gr}_{\mathbb{C}}(N_{\text{occ}}, N) = \frac{U(N)}{U(N_{\text{occ}}) \times U(N - N_{\text{occ}})}. \quad (68)$$

In this case, $\hat{\xi}_a = \hat{e}_a + \hat{e}_a^\dagger$, where

$$\hat{e}_a = \sum_{m \in \text{unocc}} \sum_{n \in \text{occ}} |u_m\rangle r_{mn}^a \langle u_n|. \quad (69)$$

This geometric structure appears in dc responses because, in the limit $\omega \ll \omega_{mn}$ for all m and n , all excitation channels contribute to the response non-trivially through the Lorentzian $i/(\omega - \omega_{mn} + i\Gamma) \sim i/\omega_{mn} \neq 0$, which on the other hand behaves as the delta function $\delta(\omega - \omega_{mn})$ that chooses a specific pair bands (m, n) for resonant frequencies. The Hermitian metric and other quantities are defined similarly. The torsion is zero.

Let us remark that the formula equation (46), used for two-level systems, applies also to the Hermitian curvature of a single state or occupied states. Instead of considering two energy levels E_n and E_m , we just need to consider two bipartite states (a single state vs the rest, or the occupied states vs the unoccupied states) and the corresponding change in the gauge group. For example, the Hermitian curvature tensor of the n th state is $K_{badc}^n = iQ_{ba}^n \mathcal{F}_{dc}^n - i\text{Tr}_{n'} Q_{dc}^{n'} \mathcal{F}_{ab}^{n'}$, where n' indicates the set of all states excluding the n th state.

We can also consider general complex flag manifolds

$$\text{Fl}_{\mathbb{C}}(N_1, \dots, N_k) = \frac{U(N)}{U(1) \times \dots \times U(N_k)} \quad (70)$$

with $\sum_{i=1}^k N_i = N$. These are all Kähler manifolds, so they have zero torsion tensor. It is straightforward to calculate the geometric quantities of the flag manifolds and their real and quaternion counterparts. One just needs to consider different gauge groups when the Maurer-Cartan form and the covariant derivative are defined.

11. First-principles calculations. We perform first-principles calculations based on the density functional theory with the generalized gradient approximation (GGA) [48]. We consider monolayer germanene modelled by a slab-supercell, ferromagnetic $(\text{LaOsO}_3)_2$ bilayer in the (111) $(\text{LaOsO}_3)_2/(\text{LaAlO}_3)_{10}$ superlattice (see [39] for the superlattice structure), and bulk Bi_2Se_3 . For germanene, the separation between two neighboring slabs is at least 15 Å in order to minimize the artificial inter-slab interaction. The electronic structure calculations are carried out using the accurate projector-augmented wave (PAW) method, as implemented in the Vienna *ab-initio* simulation package (VASP) [49, 50]. The fully relativistic PAW potentials are adopted in order to include the spin-orbit coupling (SOC) effect. Large plane-wave cutoff energies of 450 eV, 400 eV, and 350 eV are used for germanene, $(\text{LaOsO}_3)_2$ bilayer, and Bi_2Se_3 , respectively. For the Brillouin zone (BZ) integration, a k -point mesh of $20 \times 20 \times 1$, $12 \times 12 \times 2$ and $12 \times 12 \times 12$ is used respectively. All the self-consistent electronic structure calculations are performed with an energy convergence within 10^{-6} eV between the successive iterations.

The third-order injection photovoltaic Hall conductivity is calculated using Eq. (26) in Methods 3. Since a large number of k -points are needed to get accurate NLO responses [18], we use the efficient Wannier function interpolation method based on maximally localized Wannier functions (MLWFs) [51–53]. MLWFs of p orbitals for the Ge, Bi and Se atoms and d orbitals for the Os atom are constructed by fitting to the GGA+SOC band structures [Fig. 3(a,b)]. The band structures generated by the Wannier function interpolation are indistinguishable from the corresponding GGA+SOC band structures. The third-order injection current conductivity spectra [Fig. 3(c,d)] are evaluated by using dense k -meshes of $10000 \times 10000 \times 1$, $300 \times 300 \times 50$, and $400 \times 400 \times 400$ for germanene, $(\text{LaOsO}_3)_2$ bilayer, and Bi_2Se_3 , respectively. We find that the third-order conductivity obtained using such dense k -point meshes converge within a few percent. Here we consider the "cold" materials, i.e., the Fermi-Dirac function in Eq. (26) is taken to be a step function. Furthermore, the Dirac δ function is replaced by a Gaussian function with broadening width of $\varepsilon = 5$ meV. We use the relaxation rate Γ given by $\hbar\Gamma = 1$ meV.

Data Availability

The data that support the findings of this study are available from the corresponding author upon reasonable request.

[1] Thouless, D. J., Kohmoto, M., Nightingale, M. P. & den Nijs, M. Quantized Hall conductance in a two-dimensional periodic

potential. *Phys. Rev. Lett.* **49**, 405 (1982).

[2] Nagaosa, N., Sinova, J., Onoda, S., MacDonald, A. H. & Ong, N. P. Anomalous Hall effect. *Rev. Mod. Phys.* **82**, 1539 (2010).

[3] Xiao, D., Chang, M.-C. & Niu, Q. Berry phase effects on electronic properties. *Rev. Mod. Phys.* **82**, 1959 (2010).

[4] Sodemann, I. & Fu, L. Quantum nonlinear Hall effect induced by Berry curvature dipole in time-reversal invariant materials. *Phys. Rev. Lett.* **115**, 216806 (2015).

[5] Hasan, M. Z. & Kane, C. L. Colloquium: Topological insulators. *Rev. Mod. Phys.* **82**, 3045 (2010).

[6] Armitage, N. P., Mele, E. J. & Vishwanath, A. Weyl and Dirac semimetals in three-dimensional solids. *Rev. Mod. Phys.* **90**, 015001 (2018).

[7] Neupert, T., Chamon, C. & Mudry, C. Measuring the quantum geometry of Bloch bands with current noise. *Phys. Rev. B* **87**, 245103 (2013).

[8] Peotta, S. & Törmä, P. Superfluidity in topologically nontrivial flat bands. *Nat. Commun.* **6**, 8944 (2015).

[9] Xie, F., Song, Z., Lian, B. & Bernevig, B. A. Topology-bounded superfluid weight in twisted bilayer graphene. *Phys. Rev. Lett.* **124**, 167002 (2020).

[10] Lapa, M. F. & Hughes, T. L. Semiclassical wave packet dynamics in nonuniform electric fields. *Phys. Rev. B* **99**, 121111 (2019).

[11] Gao, Y. & Xiao, D. Nonreciprocal directional dichroism induced by the quantum metric dipole. *Phys. Rev. Lett.* **122**, 227402 (2019).

[12] Zhao, Y., Gao, Y. & Xiao, D. Electric polarization in inhomogeneous crystals. *Preprint at <https://arxiv.org/abs/2009.09306>* (2020).

[13] Kozii, V., Avdoshkin, A., Zhong, S. & Moore, J. E. Intrinsic anomalous Hall conductivity in non-uniform electric field. *Preprint at <https://arxiv.org/abs/2010.07322>* (2020).

[14] Gao, Y., Yang, S. A. & Niu, Q. Geometrical effects in orbital magnetic susceptibility. *Phys. Rev. B* **91**, 214405 (2015).

[15] Rhim, J.-W., Kim, K. & Yang, B.-J. Quantum distance and anomalous Landau levels of flat bands. *Nature* **584**, 59–63 (2020).

[16] de Juan, F., Grushin, A. G., Morimoto, T. & Moore, J. E. Quantized circular photovoltaic effect in Weyl semimetals. *Nat. Commun.* **8**, 15995 (2017).

[17] de Juan, F. *et al.* Difference frequency generation in topological semimetals. *Phys. Rev. Research* **2**, 012017 (2020).

[18] Ahn, J., Guo, G.-Y. & Nagaosa, N. Low-frequency divergence and quantum geometry of the bulk photovoltaic effect in topological semimetals. *Phys. Rev. X* **10**, 041041 (2020).

[19] Hosur, P. Circular photovoltaic effect on topological insulator surfaces: Berry-curvature-dependent response. *Phys. Rev. B* **83**, 035309 (2011).

[20] Morimoto, T. & Nagaosa, N. Topological nature of nonlinear optical effects in solids. *Sci. Adv.* **2**, e1501524 (2016).

[21] Nagaosa, N. & Morimoto, T. Concept of quantum geometry in optoelectronic processes in solids: Application to solar cells. *Adv. Mater.* **29**, 1603345 (2017).

[22] Holder, T., Kaplan, D. & Yan, B. Consequences of time-reversal-symmetry breaking in the light-matter interaction: Berry curvature, quantum metric, and diabatic motion. *Phys. Rev. Research* **2**, 033100 (2020).

[23] Watanabe, H. & Yanase, Y. Chiral photocurrent in parity-violating magnet and enhanced response in topological antiferromagnet. *Phys. Rev. X* **11**, 011001 (2021).

[24] Sturman, B. I. & Fridkin, V. M. *The Photovoltaic and Photo-refractive Effects in Noncentrosymmetric Materials*, vol. 8 (CRC Press, 1992).

[25] Tokura, Y. & Nagaosa, N. Nonreciprocal responses from noncentrosymmetric quantum materials. *Nat. Commun.* **9**, 3740 (2018).

[26] Boyd, R. W. *Nonlinear optics* (Academic press, 2020).

[27] Provost, J. P. & Vallee, G. Riemannian structure on manifolds of quantum states. *Commun. Math. Phys.* **76**, 289–301 (1980).

[28] Aversa, C. & Sipe, J. E. Nonlinear optical susceptibilities of semiconductors: Results with a length-gauge analysis. *Phys. Rev. B* **52**, 14636 (1995).

[29] Ventura, G., Passos, D., dos Santos, J. L., Lopes, J. V. P. & Peres, N. Gauge covariances and nonlinear optical responses. *Phys. Rev. B* **96**, 035431 (2017).

[30] Karplus, R. & Luttinger, J. Hall effect in ferromagnetics. *Phys. Rev.* **95**, 1154 (1954).

[31] Blount, E. Formalisms of band theory. In *Solid state physics*, vol. 13, 305–373 (Elsevier, 1962).

[32] Bieliavsky, P., Cahen, M., Gutt, S., Rawnsley, J. & Schwachhöfer, L. Symplectic connections. *Int. J. Geom. Methods Mod. Phys.* **3**, 375–420 (2006).

[33] Sipe, J. E. & Shkrebtii, A. I. Second-order optical response in semiconductors. *Phys. Rev. B* **61**, 5337–5352 (2000).

[34] Oka, T. & Aoki, H. Photovoltaic Hall effect in graphene. *Phys. Rev. B* **79**, 081406 (2009).

[35] Fregoso, B. M. Bulk photovoltaic effects in the presence of a static electric field. *Phys. Rev. B* **100**, 064301 (2019).

[36] Kim, H. *et al.* Accurate gap determination in monolayer and bilayer graphene/h-BN Moiré superlattices. *Nano Lett.* **18**, 7732–7741 (2018).

[37] Acun, A. *et al.* Germanene: the germanium analogue of graphene. *J. Phys. Condens. Matter* **27**, 443002 (2015).

[38] Xia, Y. *et al.* Observation of a large-gap topological-insulator class with a single Dirac cone on the surface. *Nat. Phys.* **5**, 398–402 (2009).

[39] Chandra, H. K. & Guo, G.-Y. Quantum anomalous Hall phase and half-metallic phase in ferromagnetic (111) bilayers of 4d and 5d transition metal perovskites. *Phys. Rev. B* **95**, 134448 (2017).

[40] Nakahara, M. *Geometry, Topology and Physics* (CRC Press, 2003).

[41] Allendoerfer, C. B. & Weil, A. The Gauss-Bonnet theorem for Riemannian polyhedra. *Trans. Am. Math. Soc.* **53**, 101–129 (1943).

[42] Ma, Y.-Q., Gu, S.-J., Chen, S., Fan, H. & Liu, W.-M. The Euler number of Bloch states manifold and the quantum phases in gapped fermionic systems. *EPL* **103**, 10008 (2013).

[43] Tan, X. *et al.* Experimental measurement of the quantum metric tensor and related topological phase transition with a superconducting qubit. *Phys. Rev. Lett.* **122**, 210401 (2019).

[44] Zhu, Y.-Q. *et al.* Note on “Experimental measurement of quantum metric tensor and related topological phase transition with a superconducting qubit”. *Preprint at <https://arxiv.org/abs/1908.06462>* (2019).

[45] Ma, Y.-Q. Euler characteristic number of the energy band and the reason for its non-integer values. *Preprint at <https://arxiv.org/abs/2001.05946>* (2020).

[46] Ahn, J., Kim, D., Kim, Y. & Yang, B.-J. Band topology and linking structure of nodal line semimetals with Z_2 monopole charges. *Phys. Rev. Lett.* **121**, 106403 (2018).

[47] Ahn, J., Park, S., Kim, D., Kim, Y. & Yang, B.-J. Stiefel-Whitney classes and topological phases in band theory. *Chin. Phys. B* **28**, 117101 (2019).

[48] Perdew, J. P., Burke, K. & Ernzerhof, M. Generalized gradient approximation made simple. *Phys. Rev. Lett.* **77**, 3865 (1996).

[49] Kresse, G. & Hafner, J. Ab initio molecular dynamics for liquid metals. *Phys. Rev. B* **47**, 558 (1993).

[50] Kresse, G. & Furthmüller, J. Efficient iterative schemes for

ab initio total-energy calculations using a plane-wave basis set. *Phys. Rev. B* **54**, 11169 (1996).

[51] Wang, X., Yates, J. R., Souza, I. & Vanderbilt, D. Ab initio calculation of the anomalous Hall conductivity by Wannier interpolation. *Phys. Rev. B* **74**, 195118 (2006).

[52] Marzari, N., Mostofi, A. A., Yates, J. R., Souza, I. & Vanderbilt, D. Maximally localized Wannier functions: Theory and applications. *Rev. Mod. Phys.* **84**, 1419 (2012).

[53] Ibañez-Azpiroz, J., Tsirkin, S. S. & Souza, I. Ab initio calculation of the shift photocurrent by Wannier interpolation. *Phys. Rev. B* **97**, 245143 (2018).

[54] Milnor, J. & Weaver, D. W. *Topology from the differentiable viewpoint* (Princeton university press, 1997).

[55] Nieves, J. F. & Pal, P. B. Generalized Fierz identities. *Am. J. Phys.* **72**, 1100–1108 (2004).

Acknowledgements

We appreciate Eslam Khalaf and Daniel Parker for helpful discussions and thank Maine Christos for useful comments on the manuscript. J.A. was supported by the Basic Science Research Program through the National Research Foundation of Korea (NRF) funded by the Ministry of Education (Grant No. 2020R1A6A3A03037129). J.A. and A.V. were supported by the Center for Advancement of Topological Semimetals, an Energy Frontier Research Center funded by the US Department of Energy Office of Science, Office of Basic Energy Sciences, through the Ames Laboratory under contract No. DE-AC02-07CH11358. G.-Y. G. acknowledges the support from the Ministry of Science and Technology and National Center for Theoretical Sciences in Taiwan and thanks the National Center for High-performance Computing in Taiwan for the computing time. N.N. was supported by JST CREST Grant Number JPMJCR1874 and JPMJCR16F1, Japan, and JSPS KAKENHI Grant Number 18H03676.

Competing interests

The authors declare no competing financial interests.

Additional information

Correspondence and requests for materials may be addressed to any of the authors.

Supplementary Note 1. Obstruction to finding an associated submanifold

Here, we show that there can be a topological obstruction for \hat{e}_a^{mn} to define a submanifold of $\mathcal{M} = \mathrm{U}(N)/\mathrm{U}(1)^N$. Let us first note that the complex projective line $\mathbb{C}\mathrm{P}^1 \simeq S^2$ is the only compact and closed one-dimensional complex manifold. Since $\mathbb{C}\mathrm{P}^1$ has the Euler characteristic of two, the Euler characteristic calculated in the Brillouin zone should be $\chi^{mn} = N_w \chi(\mathbb{C}\mathrm{P}^1) = 2N_w$, where N_w is the winding number of the map from the Brillouin zone to $\mathbb{C}\mathrm{P}^1$. However, our formula for the Riemann curvature tensor and the Gauss-Bonnet theorem gives

$$\begin{aligned}\chi^{mn} &= c_1^n - c_1^m \\ &= 2c_1^n - (c_1^n + c_1^m),\end{aligned}\quad (\text{S1})$$

which can be an odd integer when the total Chern number of the n and m bands is an odd number. This shows that there is a topological obstruction to defining a submanifold generated by \hat{e}_a^{mn} .

We can derive a similar result for real manifolds (PT -symmetric cases with $(PT)^2 = 1$). The real projective line $\mathbb{R}\mathrm{P}^1 \simeq S^1$ is the only compact and connected one-dimensional manifold [1]. While $\chi(\mathbb{R}\mathrm{P}^1) = 0$, meaning that $\chi^{mn} = 0$, we have in general [See Supplementary Note 3]

$$\begin{aligned}\chi^{mn} \bmod 2 &= w_1^n - w_1^m \\ &= w_1^n + w_1^m,\end{aligned}\quad (\text{S2})$$

where $w_1 = 0$ or 1 is the first Stiefel-Whitney number (Berry phase divided by π).

We can extend these to the quaternionic manifolds [$(PT)^2 = -1$]. In this case, the quaternionic projective line $\mathbb{H}\mathrm{P}^1 \simeq S^4$ has the Euler characteristic of two. So, $\chi^{mn} = N_w \chi(\mathbb{H}\mathrm{P}^1) = 2N_w$ is expected. However, an obstruction can arise due to the relation

$$\begin{aligned}\chi^{mn} &= p_1^n - p_1^m \\ &= 2p_1^n - (p_1^n + p_1^m),\end{aligned}\quad (\text{S3})$$

where p_1 is the Pontryagin number, when $p_1^n + p_1^m$ is odd.

Supplementary Note 2. Generalized Gauss-Bonnet theorem in four dimensions

The generalized Gauss-Bonnet theorem [2] in four dimensions are relevant to the case with twofold degeneracy by $(PT)^2 = -1$, in which case we have

$$\begin{aligned}\chi^{mn} &= \int dk_1 dk_2 dk_3 dk_4 \sum_{a_i, b_j} \frac{\mathrm{sgn}(\wedge^4 k)}{(2\pi)^2 2^4 2\sqrt{g}} \epsilon^{a_1 a_2 a_3 a_4} \epsilon^{b_1 b_2 b_3 b_4} \\ &\times R_{a_1 a_2 b_1 b_2}^{mn} R_{a_3 a_4 b_1 b_4}^{mn}.\end{aligned}\quad (\text{S4})$$

We show that the Euler number can be related to the difference of the Pontryagin number of bands n and m .

First, we investigate the symmetry constraints. PT symmetry $PT|u_q\rangle = G_{pq}|u_p\rangle$ imposes $(r^a)_{m_i n_j}^* = -(G^{-1} r^a G)_{m_i n_j}$. If we choose a basis where $G_{n_i n_j} = (i\sigma_y)_{n_i n_j}$ and $G_{m_i m_j} = (i\sigma_y)_{m_i m_j}$,

$$\begin{aligned}\left(r_{m_i n_j}^a \right) &= \begin{pmatrix} r_{m_1 n_1}^a & r_{m_1 n_2}^a \\ r_{m_2 n_1}^a & r_{m_2 n_2}^a \end{pmatrix} \\ &= -i f_1^a \sigma_0 + f_2^a \sigma_x + f_3^a \sigma_y + f_4^a \sigma_z,\end{aligned}\quad (\text{S5})$$

where

$$\begin{aligned}f_1^a &= \frac{i}{2} (r_{m_1 n_1}^a + r_{m_2 n_2}^a), \\ f_2^a &= \frac{1}{2} (r_{m_1 n_1}^a + r_{m_2 n_2}^a), \\ f_3^a &= \frac{i}{2} (r_{m_1 n_2}^a - r_{m_2 n_1}^a), \\ f_4^a &= \frac{1}{2} (r_{m_1 n_2}^a - r_{m_2 n_1}^a).\end{aligned}\quad (\text{S6})$$

For our purpose, it is convenient to introduce the notation

$$\begin{aligned}(r^a) &= \begin{pmatrix} 0 & 0 & r_{m_1 n_1}^a & r_{m_1 n_2}^a \\ 0 & 0 & r_{m_2 n_1}^a & r_{m_2 n_2}^a \\ r_{n_1 m_1}^a & r_{n_1 m_2}^a & 0 & 0 \\ r_{n_2 m_1}^a & r_{n_2 m_2}^a & 0 & 0 \end{pmatrix} \\ &= f_1^a \tau_y \sigma_0 + f_2^a \tau_x \sigma_x + f_3^a \tau_x \sigma_y + f_4^a \tau_x \sigma_z \\ &= f_1^a \Gamma_1 + f_2^a \Gamma_2 + f_3^a \Gamma_3 + f_4^a \Gamma_4\end{aligned}\quad (\text{S7})$$

where $\Gamma_1 = \tau_y \sigma_0$, $\Gamma_2 = \tau_x \sigma_x$, $\Gamma_3 = \tau_x \sigma_y$, $\Gamma_4 = \tau_x \sigma_z$, $\Gamma_5 = \tau_z \sigma_0$. The Gamma matrices satisfy $\Gamma_1 \Gamma_2 \Gamma_3 \Gamma_4 \Gamma_5 = 1$ and thus $\mathrm{Tr}[\Gamma_i \Gamma_j \Gamma_k \Gamma_l \Gamma_5] = 4\epsilon^{ijkl}$.

The determinant of the metric is evaluated to be.

$$g \equiv \det g^{mn} = \left(4 \sum_{a_1, a_2, a_3, a_4} \epsilon^{a_1 a_2 a_3 a_4} f_1^{a_1} f_2^{a_2} f_3^{a_3} f_4^{a_4} \right)^2. \quad (\text{S8})$$

The Riemann curvature tensor can be written simply as

$$R_{a_1 a_2 b_1 b_2}^{mn} = \frac{1}{2} \sum_{i, j} \mathrm{Tr}[F_{a_1 a_2} \mathcal{F}_{b_1 b_2}], \quad (\text{S9})$$

where we define

$$\begin{aligned}(F_{a_1 a_2}) &= \begin{pmatrix} (F_{a_1 a_2}^{nm})_{m_i m_j} & 0 \\ 0 & (F_{a_1 a_2}^{mn})_{n_i n_j} \end{pmatrix}, \\ (\mathcal{F}_{a_1 a_2}) &= \begin{pmatrix} (\mathcal{F}_{a_1 a_2})_{m_i m_j} & 0 \\ 0 & (\mathcal{F}_{a_1 a_2})_{n_i n_j} \end{pmatrix},\end{aligned}\quad (\text{S10})$$

and

$$\begin{aligned}(F_{a_1 a_2}^{mn})_{n_i n_k} &= i \sum_j (r_{n_i m_j}^{a_1} r_{m_j n_k}^{a_2} - r_{n_i m_j}^{a_2} r_{m_j n_k}^{a_1}), \\ (F_{a_1 a_2}^{nm})_{m_i m_k} &= i \sum_j (r_{m_i n_j}^{a_1} r_{n_j m_k}^{a_2} - r_{m_i n_j}^{a_2} r_{n_j m_k}^{a_1}).\end{aligned}\quad (\text{S11})$$

Therefore,

$$\begin{aligned} & \epsilon^{a_1 a_2 a_3 a_4} \epsilon^{b_1 b_2 b_3 b_4} R_{a_1 a_2 b_1 b_2}^{mn} R_{a_3 a_4 b_1 b_4}^{mn} \\ &= \frac{1}{4} \sum_{\mu, \nu, \rho, \sigma=1}^4 [\epsilon^{a_1 a_2 a_3 a_4} (F_{a_1 a_2})_{\mu \nu} (F_{a_3 a_4})_{\rho \sigma}] \\ & \times [\epsilon^{b_1 b_2 b_3 b_4} (\mathcal{F}_{b_1 b_2})_{\mu \nu} (\mathcal{F}_{b_3 b_4})_{\rho \sigma}] \end{aligned} \quad (\text{S12})$$

The FF term is

$$\begin{aligned} & \sum_{a_1, \dots, a_4} \epsilon^{a_1 a_2 a_3 a_4} (F_{a_1 a_2})_{\mu \nu} (F_{a_3 a_4})_{\rho \sigma} \\ &= - \left(4 \sum_{a_1, a_2, a_3, a_4} \epsilon^{a_1 a_2 a_3 a_4} f_1^{a_1} f_2^{a_2} f_3^{a_3} f_4^{a_4} \right) \\ & \times \sum_{i, j, k, l} \epsilon^{ijkl} (\Gamma_i \Gamma_j)_{\mu \nu} (\Gamma_k \Gamma_l)_{\rho \sigma}. \end{aligned} \quad (\text{S13})$$

Now the Gamma matrix part is

$$\begin{aligned} & \sum_{i, j, k, l} \epsilon^{ijkl} (\Gamma_i \Gamma_j)_{\mu \nu} (\Gamma_k \Gamma_l)_{\rho \sigma} \\ &= \frac{3}{2} \left[\delta_{\mu \sigma} (\Gamma_5)_{\rho \nu} + (\Gamma_5)_{\mu \sigma} \delta_{\rho \nu} - \frac{1}{2} \delta_{\mu \nu} (\Gamma_5)_{\rho \sigma} - \frac{1}{2} (\Gamma_5)_{\mu \nu} \delta_{\rho \sigma} \right] \\ &+ \frac{1}{4} \sum_{i, j, k, l} \epsilon^{ijkl} (\Gamma_i \Gamma_j)_{\mu \nu} (\Gamma_k \Gamma_l)_{\rho \sigma}, \end{aligned} \quad (\text{S14})$$

where we apply the Fierz identity twice (see A). It can be equivalently written as

$$\begin{aligned} & \sum_{i, j, k, l} \epsilon^{ijkl} (\Gamma_i \Gamma_j)_{\mu \nu} (\Gamma_k \Gamma_l)_{\rho \sigma} \\ &= 2 \left[\delta_{\mu \sigma} (\Gamma_5)_{\rho \nu} + (\Gamma_5)_{\mu \sigma} \delta_{\rho \nu} - \frac{1}{2} \delta_{\mu \nu} (\Gamma_5)_{\rho \sigma} - \frac{1}{2} (\Gamma_5)_{\mu \nu} \delta_{\rho \sigma} \right]. \end{aligned} \quad (\text{S15})$$

Using this result, we have

$$\begin{aligned} & \epsilon^{a_1 a_2 a_3 a_4} \epsilon^{b_1 b_2 b_3 b_4} R_{a_1 a_2 b_1 b_2}^{mn} R_{a_3 a_4 b_1 b_4}^{mn} \\ &= -2 \det(f_i^a) \sum_{\mu, \nu, \rho, \sigma=1}^4 \left[\delta_{\mu \sigma} (\Gamma_5)_{\rho \nu} + (\Gamma_5)_{\mu \sigma} \delta_{\rho \nu} \right. \\ & \left. - \frac{1}{2} \delta_{\mu \nu} (\Gamma_5)_{\rho \sigma} - \frac{1}{2} (\Gamma_5)_{\mu \nu} \delta_{\rho \sigma} \right] \epsilon^{b_1 b_2 b_3 b_4} (\mathcal{F}_{b_1 b_2})_{\mu \nu} (\mathcal{F}_{b_3 b_4})_{\rho \sigma} \\ &= 4 \det(f_i^a) \epsilon^{b_1 b_2 b_3 b_4} \text{Tr}(-\Gamma_5 \mathcal{F}_{b_1 b_2} \mathcal{F}_{b_3 b_4}). \end{aligned} \quad (\text{S16})$$

By combining this expression and the expression of the determinant of the metric and using $\text{sgn}[\det(f_i^a)] = \text{sgn}(\wedge^4 k)$, we finally obtain

$$\begin{aligned} \chi^{mn} &= \int dk_1 dk_2 dk_3 dk_4 \sum_{b_j} \frac{2^2}{(2\pi)^2 2^4 2} \epsilon^{b_1 b_2 b_3 b_4} \\ & \times \text{Tr}(-\Gamma_5 \mathcal{F}_{b_1 b_2} \mathcal{F}_{b_3 b_4}) \\ &= \int \frac{d^4 k}{32\pi^2} \sum_{b_j} \epsilon^{b_1 b_2 b_3 b_4} \sum_i \\ & \times [(\mathcal{F}_{b_1 b_2} \mathcal{F}_{b_3 b_4})_{n_i n_i} - (\mathcal{F}_{b_1 b_2} \mathcal{F}_{b_3 b_4})_{m_i m_i}] \\ &= p_1^n - p_1^m. \end{aligned} \quad (\text{S17})$$

Supplementary Note 3. First Stiefel-Whitney number in one dimension

Here we consider PT -symmetric systems with $(PT)^2 = 1$. Let us choose a direction a such that r_{mn}^a is nonvanishing along a one-dimensional curve in the Brillouin zone, then the first Stiefel-Whitney number on the curve is given by

$$w_1^{mn} = \frac{1}{\pi} \oint d\mathbf{k} \cdot i\partial_{\mathbf{k}} \log r_{mn}^a. \quad (\text{S18})$$

This formula is calculated in a complex smooth and periodic gauge.

The first Stiefel-Whitney number w_1^{mn} measures whether r_{mn}^a in a real gauge (where eigenstates $|n\rangle$ and $|m\rangle$ are real such that r_{mn}^a is also real) reverses its direction as it goes around the one-dimensional closed curve. To see this, since r_{mn}^a is real-valued in a real gauge, it has zero phase winding. It means that, if it had a nonzero phase winding $w_1^{mn} \neq 0$ in the smooth gauge, the gauge transformation $\{|n\rangle, |m\rangle\} \rightarrow \{e^{i\phi_n} |n\rangle, e^{i\phi_m} |m\rangle\}$ from the complex gauge to real gauge (i.e., $r_{mn}^a \rightarrow e^{-i(\phi_n - \phi_m)} r_{mn}^a$) should satisfy $\frac{1}{\pi} \oint d\mathbf{k} \cdot i\partial_{\mathbf{k}} (\phi_n - \phi_m) = w_1^{mn}$ to cancel the nontrivial phase winding. However, this kind of gauge transformation induces a nontrivial boundary condition on the real-valued tangent vector, $r_{mn}^a(2\pi) = e^{i[\phi_{nm}(2\pi) - \phi_{nm}(0)]} r_{mn}^a(0) = e^{i\pi w_1^{mn}} r_{mn}^a(0)$ in real gauge, since $r_{mn}^a(2\pi) = r_{mn}^a(0)$ in the initial complex smooth and periodic gauge. This means that r_{mn}^a in the $w_1^{mn} = 1$ case do not form a tangent vector of a real manifold, because it is not a smooth and single-valued vector on a circle.

Let us now show that w_1^{mn} can be related to topological invariants of bands n and m as in the case of the Euler characteristic of complex manifolds. That is, we show that

$$w_1^{mn} = w_1^n - w_1^m, \quad (\text{S19})$$

where w_1^n and w_1^m are the first Stiefel-Whitney numbers of bands n and m . Since w_1^n is identical to the Berry phase of band n divided by π [3, 4], i.e.,

$$w_1^n = \frac{1}{\pi} \oint d\mathbf{k} \cdot \mathcal{A}, \quad (\text{S20})$$

Eq. (S19) follows from that the real part of the following shift vector $R^{c,a} = i(r_{mn}^a)^{-1} \partial_c r_{mn}^a + (\mathcal{A}_{mm}^c - \mathcal{A}_{nn}^c)$ vanishes in PT -symmetric systems.

We can show $\text{Re}R^{c,a} = 0$ as follows. The PT symmetry constraints $PT|n\rangle = e^{i\theta_n} |n\rangle$ and $PT|m\rangle = e^{i\theta_m} |m\rangle$ lead to $r_{mn} = i|r_{mn}| e^{i(\theta_m - \theta_n)/2}$, $\mathcal{A}_{mm}^a = \frac{1}{2} \partial_a \theta_m$, $\mathcal{A}_{nn}^a = \frac{1}{2} \partial_a \theta_n$ for $m \neq n$. Therefore, we have $i(r_{mn}^a)^{-1} \partial_c r_{mn}^a = -\frac{1}{2} (\partial_c \theta_m - \partial_c \theta_n) + i|r_{mn}|^{-1} \partial_c |r_{mn}^a|$.

Appendix A: Fierz identities

Here we follow Ref. [5]. Let us introduce the notation Γ_A^μ for the 16 generators of the 4×4 matrices. Here, A indicates the representation under the action of $O(4)$, and μ indicates

the components in it.

$$\begin{aligned}\Gamma_S^{\mu=1} &= 1, \\ \Gamma_V^{\mu=1,\dots,4} &= \Gamma_\mu, \\ \Gamma_T^{\mu=1,\dots,6} &= -i\Gamma_i\Gamma_j, \\ \Gamma_A^{\mu=1,\dots,4} &= i\Gamma_5\Gamma_\mu, \\ \Gamma_P^{\mu=1} &= \Gamma_5,\end{aligned}\tag{A1}$$

where $\{\Gamma_i, \Gamma_j\} = \delta_{ij}$ for $i, j = 1, \dots, 5$.

The Fierz identity follows from the completeness of these basis matrices. That is, for any 4×4 matrix M , we can express it as

$$M = \sum_{\mu, A} m_A^\mu \Gamma_A^\mu\tag{A2}$$

for some m_A^μ . Its value given by

$$m_A^\mu = \frac{1}{4} \text{Tr}(\Gamma_A^\mu M),\tag{A3}$$

where we use (no Einstein summation convention below)

$$\text{Tr}(\Gamma_A^\mu \Gamma_B^\nu) = 4\delta_{\mu\nu} \delta_{AB}.\tag{A4}$$

Rewriting the above completeness relation,

$$\begin{aligned}M_{ab} &= \sum_{\mu, A} \frac{1}{4} \text{Tr}(\Gamma_A^\mu M)(\Gamma_A^\mu)_{ab} \\ &= \frac{1}{4} \sum_{\mu, A} \sum_{c, d} (\Gamma_A^\mu)_{cd} M_{dc} (\Gamma_A^\mu)_{ab} \\ &= \sum_{c, d} \left[\frac{1}{4} \sum_{\mu, A} \Gamma_A^\mu \Gamma_A^\mu \right]_{ab; cd} M_{dc},\end{aligned}\tag{A5}$$

one can find

$$\frac{1}{4} \sum_{\mu, A} (\Gamma_A^\mu)_{ab} (\Gamma_A^\mu)_{cd} = \delta_{ad} \delta_{bc}.\tag{A6}$$

Let us multiply $(\Gamma_B^\nu)_{b'b} (\Gamma_B^\nu)_{d'd}$ and sum over ν, a, c .

$$\begin{aligned}& \sum_{\nu} (\Gamma_B^\nu)_{ad'} (\Gamma_B^\nu)_{cb'} \\ &= \frac{1}{4} \sum_{\mu, \nu, A} (\Gamma_A^\mu \Gamma_B^\nu)_{ab'} (\Gamma_A^\mu \Gamma_B^\nu)_{cd'} \\ &= \sum_{\rho, \sigma, C} (\Gamma_C^\rho)_{ab'} (\Gamma_C^\sigma)_{cd'} \left(\frac{1}{4} \sum_{\mu, \nu, A} f_{CAB}^{\rho\mu\nu} f_{CAB}^{\sigma\mu\nu} \right) \\ &= \sum_{\rho, C} (\Gamma_C^\rho)_{ab'} (\Gamma_C^\rho)_{cd'} K_{BC},\end{aligned}\tag{A7}$$

where we use that $\sum_{\mu, \nu, A} f_{CAB}^{\rho\mu\nu} f_{CAB}^{\sigma\mu\nu} \propto \delta_{\rho\sigma}$ because it should be $O(4)$ -invariant. The value of K can be calculated by contracting a with b' and c with d' :

$$\text{Tr}(\Gamma_B^\nu \Gamma_D^\sigma \Gamma_B^\nu \Gamma_D^\sigma) = \sum_{\rho, C} [\text{Tr}(\Gamma_C^\rho \Gamma_D^\sigma)]^2 K_{BC} = 16 K_{BD}\tag{A8}$$

So,

$$K_{AB} = \frac{1}{16} \sum_{\mu, \nu} \text{Tr}(\Gamma_A^\mu \Gamma_B^\nu \Gamma_A^\mu \Gamma_B^\nu).\tag{A9}$$

$$(K_{AB}) = \frac{1}{4} \begin{pmatrix} 1 & 1 & 1 & 1 & 1 \\ 4 & -2 & 0 & 2 & -4 \\ 6 & 0 & -2 & 0 & 6 \\ 4 & 2 & 0 & -2 & -4 \\ 1 & -1 & 1 & -1 & 1 \end{pmatrix}.\tag{A10}$$

[1] J. Milnor and D. W. Weaver, *Topology from the differentiable viewpoint* (Princeton university press, 1997).
[2] C. B. Allendoerfer and A. Weil, The Gauss-Bonnet theorem for Riemannian polyhedra, *Trans. Am. Math. Soc.* **53**, 101 (1943).
[3] J. Ahn, D. Kim, Y. Kim, and B.-J. Yang, Band topology and linking structure of nodal line semimetals with Z_2 monopole charges, *Phys. Rev. Lett.* **121**, 106403 (2018).
[4] J. Ahn, S. Park, D. Kim, Y. Kim, and B.-J. Yang, Stiefel-Whitney classes and topological phases in band theory, *Chin. Phys. B* **28**, 117101 (2019).
[5] J. F. Nieves and P. B. Pal, Generalized fierz identities, *American journal of physics* **72**, 1100 (2004).